台灣顯微鏡學會

第三十七屆學術研討會 106年6月24日 國立台灣大學

JEOL 日本電子株式会社
捷東股份有限公司
Solutions for Innovation

"NEOARM"

New Atomic Resolution Analytical Electron Microscope

Ultimate Resolution powered by "Neo Engine" -
Cold FEG with NEO ASCOR(Advanced STEM Cs corrector)

Ultimate Resolution
Challenge to 60 pm

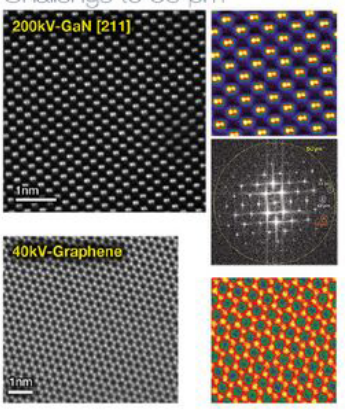

Enhanced light atom contrast
e-ABF

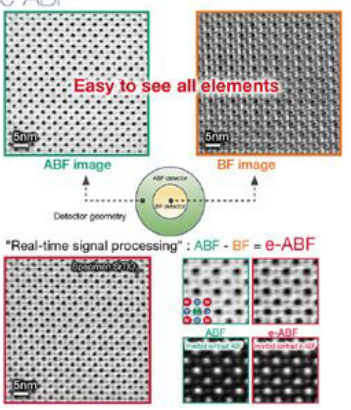

Easy to Tune Cs
JEOL COSMO™ Tune

Automated Aberration tuning
including Higher order (up to 4th order)

Fast and **accurate** tuning
with no standard sample

Operate microscope in a bright room
Desktop EM

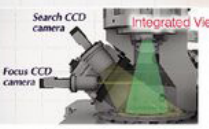

Camera for the viewing chamber is equipped as standard.
Sample search, microscope alignment....,
all is doable just by looking at a PC monitor.

Resolution	STEM HAADF Image	70 pm (200 kV), 100 pm (80 kV), 160 pm (30 kV)
	TEM information limit	100 pm (200 kV), 110 pm (80 kV), 250 pm (30 kV)
Electron gun	Cold field emission gun -standard	
Aberration corrector	STEM: NEO ASCOR HOAC , TEM: CETCOR with DSS	
Corrector auto tuning system	NEO JEOL COSMO™ auto tuning system, Ad-hock tune (SIAM)	
Accelalation voltage	30 to 200 kV (30, 80, 200 kV -standard, 60, 120 kV -option)	
Magnetic field free mode	Lorentz lens settings (x50 to 80 k on screen) -standard	
Specimen movement system	X, Y and Z super fine mecanical drives, ultra fine piezo device drives -standard	
Oparation type	RDS operation	

主辦單位:台灣顯微鏡學會　協辦單位:台灣大學材料科學與工程學系

MA-tek The Best R&D Partner

Founded in 2002, Materials Analysis Technology Inc. (MA-tek) is a leading laboratory in materials analysis (MA). Accompanying with the fast growing pace of business develop0ment, MA-tek has successfully expanded to provide Failure Analysis (FA) and Reliability Testing (RT) services as well, which is superior integrated service for customers in various industries. Up to now, MA-tek has set up 6 laboratories and 1 sales office worldwide, providing around-the clock services in logistic support and technical services.

Our Service Items

Project Based Services

- Training Courses, Lectures
- IP strategic planning
- Patent infringement study
- Benchmark study
- Competitors Analysis
- Design Services

MA / PFA

- Decap, Delayer, Parallel lapping
- SEM / EDX
- TEM / EDX / EELS
- FIB, Circuit editing
- SIMS, SRP
- Auger, XPS, XRD
- Optical profiler
- SCM, AFM
- FTIR, Raman

EFA / ESD

- X-ray radiography
- SAT
- EMMI / InGaAs, OBIRCH
- Themos-mini
- C-AFM
- Passive voltage contrast
- ESD / Latch-up testing
- Wire bonding, packaging

Reliability Tests

- HAST, LTST
- THST, PCT / UB-HAST
- TCT, TST
- HTOL, BLT, ELFR
- Reflow Test

◆ Case log-in, please contact: sales@ma-tek.com / +886 3 611 6678 ext.3821 / www.ma-tek.com

Bio Ma-tek

Bio Materials Analysis Technology Inc. (Bio Ma-tek) address the ever demanding needs on the physical and chemical characterization of nano materials in biological systems, Bio Ma-tek rolls out an array of bio-EM sample preparation and image analysis services and a comprehensive list of analytical services following the recommendations in ISO/TR13014.

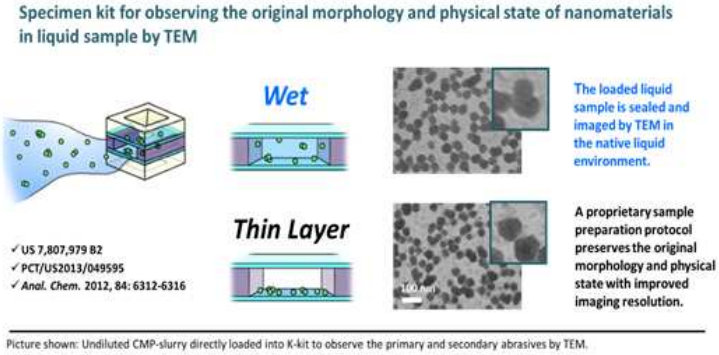

Liquid Sample TEM

- Liquid Sample TEM Service and Sales
- Bio-sample and Bio-materials EM Specimen Preparation
- Other Electron Microscopy Analysis：Liquid、Cryo、Gel、Solid、etc.

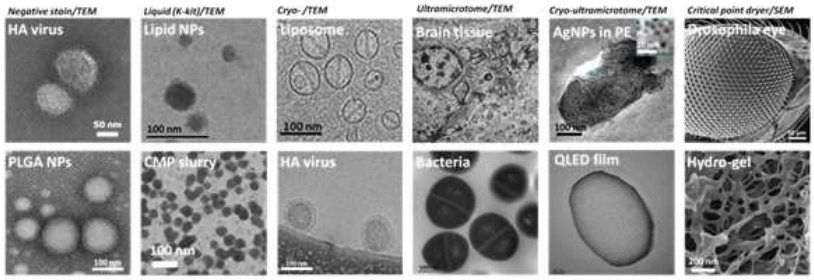

Other TEM Specimen Preparation

Bruker Singapore Pte. Ltd.
11 Biopolis Way #10-10
The Helios, Singapore 138667
Phone +65 6500 7288
Fax +65 6500 7289
info.bna.sg@bruker.com
www.bruker.com

BRUKER

EDS, WDS, EBSD, Micro-XRF and Micro-CT - five analysis methods for SEM from a single source.

- QUANTAX EDS: provides highest energy resolution and maximum throughput
- QUANTAX WDS: offers maximum sensitivity in the low energy range
- QUANTAX EBSD: sets new standards in combined EBSD/EDS
- XTrace: adds Micro-XRF analysis capabilities to the SEM
- Micro-CT for SEM: reveals the internal microstructure of samples

Someone has to be first.

台灣顯微鏡學會

Microscopy Society of Taiwan

第三十七屆年會廠商贊助

JDC

JEOL

OXFORD INSTRUMENTS

MA-tek

FEI

part of Thermo Fisher Scientific

GATAN

BRUKER

SANPANY

tsmc

台灣積體電路製造股份有限公司

iST INTEGRATED SERVICE TECHNOLOGY

Leica MICROSYSTEMS

CAMECA SCIENCE & METROLOGY SOLUTIONS

AMETEK MATERIALS ANALYSIS DIVISION

FISCHIONE INSTRUMENTS

TOMOCUBE, INC.

EBT

目錄

第三十七屆臺灣顯微鏡學會年會

106 年 6 月 24 日(星期六) 國立臺灣大學博理館

08:30-09:30	報到
09:30-10:00	開幕儀式與理事長報告
10:00-10:30	材料物理邀請演講：Dr. Torranin Chairuangsri President of the Microscopy Society of Thailand
10:40-11:10	生物醫學邀請演講：中國醫藥大學附設醫院病理部部主任 王約翰醫師
11:20-12:00	台灣顯微鏡學會會員大會 討論提案： 1. 通過 106 年度工作報告、收支決算表 2. 通過 2017 年第三屆東亞顯微鏡國際研討會在韓國舉行，本會舉派演講者名單。
12:00-13:30	午餐時間 (備有午餐餐盒) Poster Session (地點：一樓大廳)
	專題演講
13:00-13:30	**Low dose observation of pseudo atomic column elemental maps by 2D STEM moiré method with dual detector EDS system** Mr.Yukihito Kondo/ JEOL Ltd.
13:30-14:00	**Atomic resolution TEM imaging of metal-organic frameworks (MOFs) by using direct detection and electron counting** Dr.Ming Pan/ Gatan Inc.
14:00-14:20	**How to make your current TEM performance upgraded** 林坤興先生/ Thermo Fisher Scientific Application manager
14:20-14:40	**Advanced Applications using an annular four-channel Silicon Drift Detector** A. Wong/ Bruker
14:40-15:00	**SYMMETRY- New Generation EBSD detector** 王廷玉/ Oxford Instruments
15:00-16:00	廠商商展及討論交流時間（備有點心茶點 ） 海報解說 (地點：一樓大廳)
16:00-16:20	公布第十八屆理、監事選舉結果
16:20-16:40	論文海報與攝影比賽獲獎作品導覽
16:40-17:00	頒獎、閉幕

台灣顯微鏡學會

第十七屆理、監事名錄

理 事 長	楊哲人	台灣大學材料科學與工程學系	教授
副理事長	陳香君	台灣大學生命科學系	教授
副理事長	李志浩	清華大學工程與系統科學系	教授
常務理事	劉康庭	友聯光學股份有限公司	董事長
	謝詠芬	閎康科技股份有限公司	董事長
	薛景中	中央研究院應用科學研究中心	副研究員
理　　事	朱明文	台灣大學凝態中心	研究員
	陳福榮	清華大學工程與系統科學系	教授
	張　立	交通大學材料科學與工程學系	教授
	蘇紘儀	台灣積體電路有限公司	故障分析處處長
	劉全璞	成功大學材料科學與工程系	教授
	孫啟光	台灣大學電機工程學系	教授
	簡萬能	中央研究院植物暨微生物學研究所	研究技師
	高甫仁	陽明大學生醫光電研究所	教授
	陳金富	捷東股份有限公司	總經理
侯補理事	胡宇光	中央研究院物理研究所	研究員
	鄭貽生	國立台灣大學植物科學研究所	教授
	薛富盛	國立中興大學校長/材料科學與工程學系	教授
	王星豪	國立臺灣海洋大學機械與機電工程學系	教授
	王建義	國立東華大學材料科學與工程學系	教授
	蔡定平	台灣大學物理系	教授
	章為皓	中央研究院化學研究所	副研究員
常務監事	鮑忠興	宜特科技	顧問
	周苡嘉	國立交通大學電子物理系	教授
	林招松	台灣大學材料科學與工程學系	教授
	江安世	清華生命科學院	教授
	許秋容	中興大學生命科學系	教授
候補監事	曾傳銘	明志科技大學材料工程系	教授
	謝達斌	國立成功大學基礎醫學研究所	教授

PLENARY SPEECH

Electron Microscopy Study of Multiple Carbides in Cr-Mo White Cast Irons

T. Chairuangsri[1], S. Nusen[1], S. Imurai[2], A. Wiengmoon[3] and J.T.H. Pearce[4]

[1]Department of Industrial Chemistry, Chiang Mai University, Chiang Mai 50200, Thailand

[2]Faculty of Science and Technology, Rambhai Barni Rajabhat University, Chanthaburi 22000, Thailand

[3]Department of Physics, Faculty of Science, Naresuan University, Phitsanulok 65000, Thailand

[4]Panyapiwat Institute of Management, Nonthaburi 11120, Thailand

tchairuangsri@gmail.com

Corrosive/abrasive wear of high Cr white cast irons (HCCIs) depends on carbide type and morphology within their microstructure. As-cast 28Cr HCCIs with Mo addition and relatively high Cr/C ratio about 10 are of interest because of their potentially good resistance to corrosive/abrasive wear in acidic slurries. Recently, we have reported effects of Mo on microstructure of as-cast 28Cr–2.6C with up to 10wt.% Mo addition by means of electron microscopy. Mo addition promoted the formation of $M_{23}C_6$ and M_6C, consequently complex carbides were found within dominantly austenitic matrices. Three types of carbides, including M_7C_3 (about 1000-1800 HV), $M_{23}C_6$ (about 1000 HV) and M_6C (about 1200–1800 HV), were identified, where $M_{23}C_6$ localized as a transition zone between M_7C_3 and M_6C. Distinctive characteristics of M_7C_3 are faulting and streaking in electron diffraction pattern, whereas those of M_6C are the strongest backscattered electron signal and relatively high Mo and Si content. In the present study, multiple carbides in as-cast hypoeutectic 28Cr–2.6C-(0 to 6)Mo HCCIs were further investigated by means of scanning electron microscopy (SEM) and transmission electron microscopy (TEM). Formation and crystallographic study of these as-cast multiple carbides in HCCIs will be discussed.

Keywords: Electron Microscopy, Carbides, High Chromium Cast Irons, White Cast Irons

รองศาสตราจารย์ ดร. ธรณินทร์ ไชยเรืองศรี

Associate Professor Dr. Torranin Chairuangsri

Department of Industrial Chemistry, Faculty of Science,
Chiang Mai University, Chiang Mai, 50200 Thailand
Tel: +66-53-943301
Fax: +66-53-222268
E-mail: **tchairuangsri@gmail.com**

EDUCATIONAL BACKGROUND

1994-1998	PhD (Metallurgy) University of Leeds, UK
1989-1993	B.S. (Industrial Chemistry) Chiang Mai University, Chiang Mai, Thailand

POSITIONS

2017-present	Dean, Faculty of Science, Chiang Mai University
2014-present	President, The Microscopy Society of Thailand (MST)
2015-2017	Associate Dean for Academic Affairs, Faculty of Science, Chiang Mai University
2006-2014	Head, Department of Industrial Chemistry, Chiang Mai University

FIELDS OF SPECIALIZATION

- Transmission Electron Microscopy
- Physical Metallurgy

AWARDS

2014	Outstanding Thailand Metallurgist, The Committee of the 8th Thailand Metallurgy Conference, 2014, Bangkok, Thailand
2009	Young Asian Electron Microscopist Award, The 65th Annual Meeting of the Japanese Society of Electron Microscopy, May 26-29, 2009, Sendai, Japan.
2005	“Chang-Tong-Kam” Medal for Outstanding Young Researcher, Chiang Mai University, Thailand
2004	Certificate, Outstanding Researcher Among New Scholars, The Thailand Research Fund (TRF) and The Commission of Higher Education, Thailand
2003	Outstanding Research Unit, Faculty of Science, Chiang Mai University, Thailand

SELECTED PUBLICATIONS (2011-present)

1. A. Wiengmoon, J.T.H. Pearce, S. Nusen, T. Chairuangsri, Effects of Si on microstructure and phase transformation at elevated temperatures in ferritic white cast irons, Materials Characterization 120 (2016), 159-167. (IF 2015 = 2.383).
2. N. Jantaping, C. Banjongprasert, T. Chairuangsri, U. Patakham, Y. Boonyongmaneerat. Challenges and strategies of surface modification of electrogalvanized coatings for electron microscopy analysis. Micron 86 (2016), 48–53. (IF 2016 = 1.838)
3. S. Nusen, T. Chairuangsri, Z. Zhu, C.Y. Cheng, Recovery of indium and gallium from synthetic leach solution of zinc refinery residues using synergistic solvent extraction with LIX 63 and Versatic 10 acid, Hydrometallurgy. 160 (2016) 137–146. (IF 2014 = 1.933).
4. A. Wiengmoon, P. Sukchot, N. Tareelap, J.T.H. Pearce, T. Chairuangsri, Effects of T6 Heat Treatment with Double Solution Treatment on Microstructure, Hardness and Corrosion Resistance of Cast Al-Si-Cu Alloy, Arch. Metall. Mater. 60 (2015) 881–886. (IF 2014 = 1.090).
5. S. Imurai, C. Thanachayanont, J.T.H. Pearce, T. Chairuangsri, Microstructure and Erosion-Corrosion Behaviour of as-Cast High Chromium White Irons Containing Molybdenum in Aqueous Sulfuric-Acid Slurry, Arch. Metall. Mater. 60 (2015) 919–923. (IF 2014 = 1.090).
6. C. Banjongprasert, A. Jak-Ra, C. Domrong, U. Patakham, W. Pongsaksawad, T. Chairuangsri, Characterization of An Equal Channel Angular Pressed Al-Zn-In Alloy, Arch. Metall. Mater. 60 (2015) 887–890. (IF 2014 = 1.090).
7. M. Thepnurat, T. Chairuangsri, N. Hongsith, P. Ruankham, S. Choopun, Realization of Interlinked ZnO Tetrapod Networks for UV Sensor and Room-Temperature Gas Sensor, ACS Appl. Mater. Interfaces. 7 (2015) 24177–24184. (IF 2014 = 6.723).
8. S. Nusen, Z. Zhu, T. Chairuangsri, C.Y. Cheng, Recovery of germanium from synthetic leach solution of zinc refinery residues by synergistic solvent extraction using LIX 63 and Ionquest 801, Hydrometallurgy. 151 (2015) 122–132. (IF 2014 = 1.933).
9. S. Imurai, C. Thanachayanont, J.T.H. Pearce, K. Tsuda, T. Chairuangsri, Effects of W on microstructure of as-cast 28 wt.%Cr-2.6 wt.%C-(0-10) wt.%W irons, Mater. Charact. 99 (2015) 52–60. (IF 2014 = 1.845).
10. S. Imurai, C. Thanachayanont, J.T.H. Pearce, K. Tsuda, T. Chairuangsri, Effects of Mo on microstructure of as-cast 28 wt.% Cr-2.6 wt.% C-(0-10) wt.% Mo irons, Mater. Charact. 90 (2014) 99–112. (IF 2014 = 1.845).
11. A. Wiengmoon, J.T.H. Pearce, T. Chairuangsri, S. Isoda, H. Saito, H. Kurata, HRTEM and HAADF-STEM of precipitates at peak ageing of cast A319 aluminium alloy, Micron. 45 (2013) 32–36. (IF 2014 = 1.988).
12. S. Nusen, N. Yottawee, S. Daopiset, T. Chairuangsri, The role of surface grinding, intermetallic precipitates and halide ions on zinc deposition and adhesion on aluminium cathode in zinc electrowinning, Hydrometallurgy. 113 (2012) 143–154. (IF 2014 = 1.933).
13. A. Wiengmoon, J.T.H. Pearce, T. Chairuangsri, Relationship between microstructure, hardness and corrosion resistance in 20 wt.%Cr, 27 wt.%Cr and 36 wt.%Cr high chromium cast irons, Mater. Chem. Phys. 125 (2011) 739–748. (IF 2014 = 2.259).
14. P. Dechkrong, S. Jiwajinda, P. Dokchan, M. Kongtungmon, N. Chomsaeng, T. Chairuangsri, C.C. Yuf, C.N. Hsiaof, M. Shiojiri, Fine structure of wing scales of butterflies, Euploea mulciber and Troides aeacus, J. Struct. Biol. 176 (2011) 75–82. (IF 2014 = 3.231).
15. P. Chindaprasirt, K. Boonserm, T. Chairuangsri, W. Vichit-Vadakan, T. Eaimsin, T. Sato, K. Pimraksa, Plaster materials from waste calcium sulfate containing chemicals, organic fibers and inorganic additives, Constr. Build. Mater. 25 (2011) 3193–3203. (IF 2014 = 2.296).

中國醫藥大學附設醫院病理部部主任

王約翰醫師

學歷：

國防醫學院　醫學士　醫學系
國防醫學院　碩士　病理學研究所
國防醫學院　博士　醫學研究所

經歷：

三軍總醫院病理部　住院醫師/住院總醫師/主治醫師
國軍八一七醫院檢驗科　科主任
國軍花蓮總醫院病理部　部主任
嘉義榮民醫院醫學檢驗科　科主任
台中榮民總醫院病理檢驗部　部主任

Leica
MICROSYSTEMS

EM AFS2: Freeze Substitution

EM GP: Automatic plunge Freezing

EM ACE: sample Coater

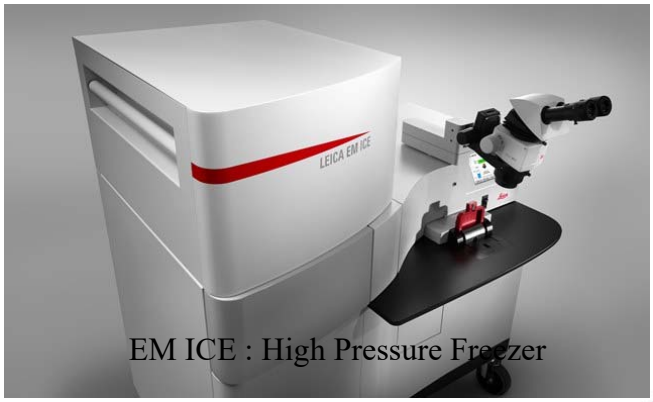

EM ICE : High Pressure Freezer

EM TRIM2: EM Trimming device

EM CPD300: critical point dryer

EM TP: EM tissue processing

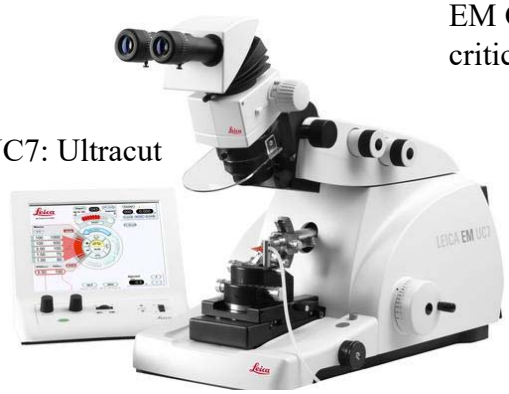

EM UC7: Ultracut

EM UC7+FC7: Freexing Ultrcut

友聯光學有限公司 UNION OPTICAL
Tel:(02)2698-0508 E-mail: unionopt@ms11.hinet.net

pub_taiwan_sem2017-LEAP-eikos_Mise en page 1 24/05/2017 10:19 Page 1

CAMECA
SCIENCE & METROLOGY SOLUTIONS

nu

AMETEK
MATERIALS ANALYSIS DIVISION

LEAP® 5000
Atom Probe

The **LEAP 5000** provides unmatched 3-dimensional subnanometer compositional information across a wide variety of metals, semiconductors and insulators.

- Optimum analysis volumes and detection efficiency
- Unparalleled compositional precision and accuracy
- High productivity.

Also in our Atom Probe Tomography (APT) product line, the **EIKOS**™ Atom Probe offers increased ease-of-use and a low cost-of-ownership, enabling routine 3D nano-analysis for both research and industry.

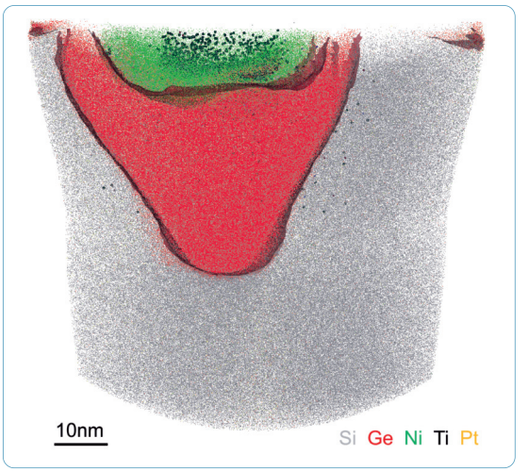

3D analysis of the source-drain region of a 28nm transistor revealing titanium and platinum doping in the nickel silicide to SiGe contact.

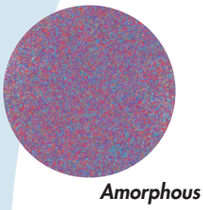

Amorphous materials

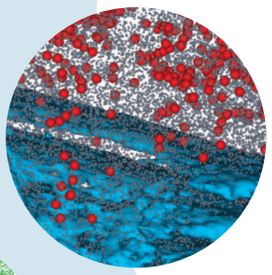

InGaN LED structures

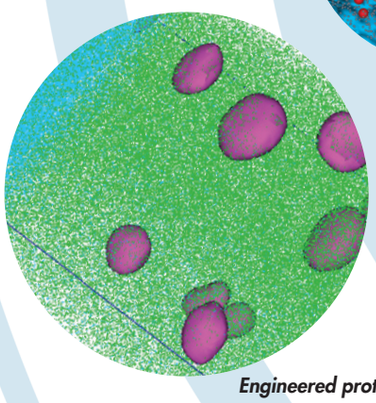

Engineered protective oxides

Visit **www.cameca.com/new/leap-applications.aspx**
to receive a full set off LEAP application notes.

Your contact in Taiwan: cameca.taiwan@ametek.com • Phone +886 3 5750099

Low dose observation of pseudo atomic column elemental maps by 2D STEM moiré method with dual detector EDS system

Yukihito Kondo(近藤行人)[1], Kei-ichi Fukunaga(福永啓一)[1], Eiji Okunishi(奥西栄治)[1] and Noriaki Endo(遠藤徳明)[1]

1. JEOL Ltd., 3-1-2 Musashino, Akishima, Tokyo 196-8558, Japan
*kondo@jeol.co.jp

Atomic column elemental mapping, by energy dispersive X-ray spectrometry (EDS), is a powerful for materials research, since elements and sites are determined simultaneously. The sample damage is a key to be overcome, because the EDS signal is small. We have developed a new dual detector system to enhance the sensitivity [1]. However, there are many materials, which suffer damage even with the new detector. Recently, we have applied the 2D STEM moiré method to obtain a pseudo atomic column map [2]. With this method, the electron density is greatly reduced to be < 1 % of one for the conventional method, since a pixel interval is much sparse. In this paper, we compare the damages of a Si_3N_4 sample on the atomic elemental column maps obtained by conventional and 2D STEM moiré methods.

In our experiment, we used an aberration corrected microscope (JEOL, JEM-ARM200F) equipped with a CFEG and the new SDD system (solid angle = 1.75 sr). The sample used was Si_3N_4 (hexagonal structure with $\boldsymbol{a} = \boldsymbol{b}$ = 0.7617 nm and **c** = 0.291 nm). Figure 1 shows the atomic column elemental maps by the 2D moiré and conventional methods. The peaks in the Si map in both maps accord well with the atomic sites expected from the sample crystal structure. However, the peaks in N map accord with the atomic sites only in the 2D moiré map. The difference between N maps by two methods is thought to be originated from the dose density. The reduced rate of the dose density by the 2D moiré method was 1/320 to the direct method. The results clearly show the affection of dose density by comparing the pseudo 2D moiré atomic column elemental maps with a direct map.

References

[1] S. Kawai *et al*, Microsc. Microanal. **20 (S3)** (2014) p.1150.

[2] Y. Kondo and E. Okunishi, Microscopy **63 (5)** (2014), **p.** 391.

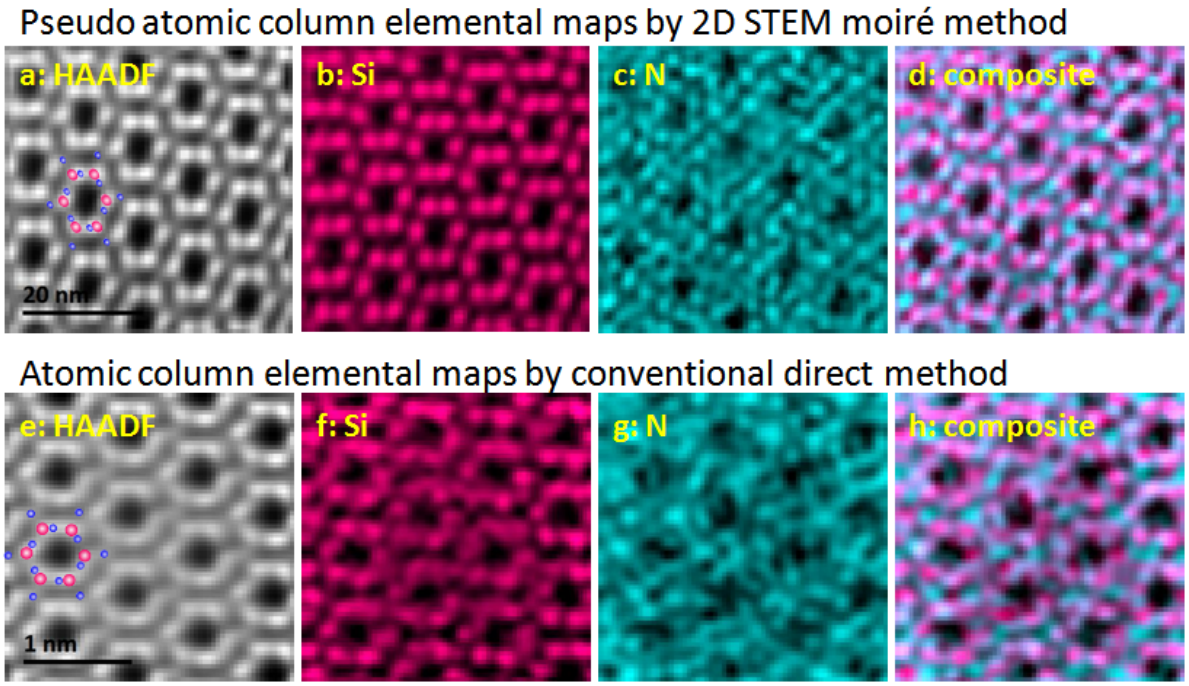

Figure 1. *(a-d) show the HAADF, Si map, N map and composite map of Si and N by 2D moiré method, and (e-h) are those by direct mapping. The dose density is greatly reduced in 2D moiré maps, since the scanned area is large because of sparse pixel interval. The results were obtained under the conditions: acc. Volt. = 120 kV, probe current = 38 pA, probe size = 0.2 nm.*

Atomic resolution TEM imaging of metal-organic frameworks (MOFs) by using direct detection and electron counting

Ming Pan
Gatan, Inc., Pleasanton, CA, USA

Metal-organic frameworks (MOFs) are a new class of materials that has attracted world-wide attention [1] in recent years for their vast potential in industrial applications such as environmental, gas separation, storage and purification, ion conduction, catalysis, membranes, etc. MOFs are crystalline porous materials with designable topology, porosity and functionality. Compared with other microporous materials such as zeolites, meso-porous silica and porous carbon, MOFs have significantly larger surface areas and internal cavities for gas adsorption. Structure characterization is important to understand the property and functionality of MOFs.

Diffraction based techniques (e.g. x-ray and electron) are widely used to determine the structures. However, surface, defects and interfaces are believed to play an equally important role as the average crystal structures in understanding the structure-roperty-functionality relationship. High resolution transmission electron microscopy (HRTEM) is the only technique that is capable of providing high resolution or even atomic resolution structural information on not only the average structures but more importantly on surface, defects and interfaces.

Like other porous materials, MOFs are extremely sensitive to electron beam irradiation. Under normal imaging conditions, the structures of MOFs would be destroyed instantly making it impossible to image the pristine structures. For this reason, very few high resolution images of MOFs have been reported to date and none at atomic resolution. A new generation image device in direct detection and electron counting [2] has achieved tremendous success in single particle cryoEM [3-4], thanks to its extreme sensitivity and high resolution.

In this presentation, the state-of-the-art direct detection electron counting cameras will be described and shown to have major impact in TEM imaging of pristine MOF structures at atomic resolution [5].

References

1. Furukawa, H., Cordova, K.E., O'Keeffe, M., Yaghi, O.M., Science, 2013, Vol. 341, 1230444. doi: 10.1126/science.1230444.
2. Li, X.; Mooney, P.; Zheng, S.; Booth, C.R.; Braunfeld, M.; Gubbens, S.; Agard, D.A.; Cheng, Y., Nature Methods, 2013,10, 584-590. doi:10.1038/nmeth.2472.
3. Merk, A.; Bartesaghi, A; Banerjee, S.; Falconieri, V.; Rao, P.; Davis, M.I.; Pragani, R.; Boxer, M. B.; Earl, L.A.; Milne, J.L.S.; Subramaniam, S., Cell, 2016, 165, Iss. 7, 1698-1707. doi:10.1016/j.cell.2016.05.040.
4. Yan, C.; Wan, R.; Bai, R.; Huang, G.; Shi, Y., Science, 2017, 355 (6321), 149-155.
5. Zhu, Y.; Ciston, J.; Zheng, B.; Miao, X.; Czarnik, C.; Pan, Y.; Sougrat, R.; Lai, Z.; Hsiung, C.; Yao, K.; Pinnau, I.; Pan, M.; Han, H., Nature Materials, 2017, 16, 532-537. doi: 10.1038/NMAT4852.

Advanced Applications using an annular four-channel Silicon Drift Detector

Max Patzschke[1*], Andi Käppel[1,], Igor Nemeth [1] A. Wong [1]

[1] Bruker Nano GmbH, Am Studio 2D, 12489 Berlin, Germany

*Corresponding author, e-mail: alex.wong@bruker.com

Keywords: *EDS, FlatQuad, high speed mapping, no shadowing effects, high input count rate*

Abstract

Special configuration has been recently developed for certain applications in order to improve certain limitations:

A special multi element concept is the XFlash® 5060FQ, an annular detector which can be placed between the pole piece and the sample in a standard SEM. The four SDD elements have an active area of 15 mm² each resulting in a total of 60 mm². This large active area and the annular geometry, where the detector elements are very close to the x-ray source, lead to an extremely large solid angle of more than 1 sr. This is a value which is typically 100 times larger than a 10 mm² detectors in a conventional setup. Therefore extremely high count rates can be achieved easily even with low probe currents, and can be processed with four separate electronic channels in parallel, leading to maximum output count rate of more than 1,100,000 cps [1,2].

These properties make the detector an ideal device for high speed mappings, sensitive samples and his relatively high take-off angle lead to a significant reduction of shadowing effects on rough surfaces. Examples benefiting from these latest developments will be presented.

References:

[1] H. Soltau et al., Microsc. Microanal. 15 (Suppl.2) (2009), 204

[2] R. Terborg, M. Rohde, Microsc. Microanal. 17 (Suppl.2) (2011), 892

SYMMETRY- New Generation EBSD detector

王廷玉
Oxford Instruments

Symmetry, the world`s first EBSD detector based on CMOS sensor technology, is set to revolutionize EBSD analysis. Operating at over 3,000 indexed patterns per second(pps), Symmetry balances unprecedented speed with exceptional sensitivity to enable work even at low beam currents and voltages. All of this is delivered within a design that provides perfect operational simplicity. Now you can use a single detector for all applications - with no compromise.

台灣積體電路製造股份有限公司
Taiwan Semiconductor Manufacturing Company, Ltd.

2017 TSMC CAMPUS JOB FAIR

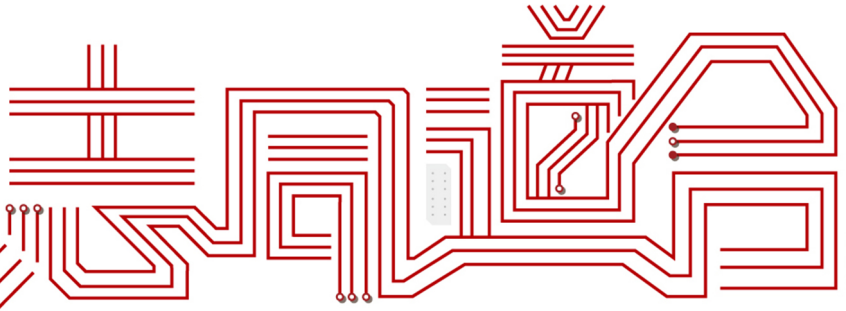

台積電　校園徵才

Unleash Innovation, Amplify Potential

尋找「志同道合」的你，一起開創全球半導體業
無限可能，現在就透過專屬網頁完成履歷投遞，
符合資格者，可享有優先面試機會喔！

填寫履歷

WE WANT YOU

- 大學(含)以上且無兵役義務，可於2017年報到就職
- 主修電機(子)、光電、物理、材料、化學(工)、機械、資工(管)、工工、財會、管理、人資、勞工關係、心理相關科系

HT-1

無螢光標記活細胞4D成像顯微鏡
Label-Free 4D Holographic Microscope

1). HT-1 採用最新一代的鐳射掃描的全息成像與斷層掃描技術 (Holograph & Tomograph)

2). HT-1 是高速, 高解析, 即時斷層掃描, 無需螢光標記的活細胞3D/4D成像顯微鏡. 也包括應用于組織成像, 動態成像與定量量測分析.

3). 可選擇 60x/0.8 或 60x/1.2 水鏡.

4). 最高成像解析 XY/Z : 110/356 納米, 視野/厚度 : 80/40 微米

5). 高速3D 成像速率 > 2.5 fps.
長時間活細胞4D成像 > 72 小時.

6). 樣本無須染色, 包括活細胞與組織.

7). 獨家創新DMD技術, 無須轉動光學鏡組, 保證系統的精准度與穩定度.

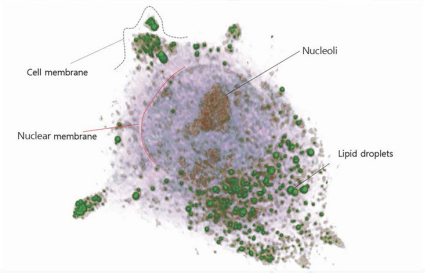

全息影像 / 無須螢光標記 / 低功率雷射掃描 / 快速成像 / 超高解析 / 長時間影像擷取 / 定量分析 / 應用廣泛

TOMOCUBE, INC.

請洽 :
美嘉儀器股份有限公司
www.major.com.tw
TEL : 02-2808-1452

第三十七屆臺灣顯微鏡學會年會研討會

材料物理與生物醫農組　論文海報競賽

材料物理組		
A-01	**Conversion of ZnS into Cu2-xS superlattice in one-dimensional nanostructure through cation exchange reactions** [1]Chi-Lin Tsai(蔡季霖) and [1]Chuan-Pu Liu(劉全璞) Department of Materials Science and Engineering, National Cheng Kung University, Tainan 70101, Taiwan	16
A-02	**In-situ HRTEM investigation of the separated nucleation in the AA7050 aluminium alloy** Tsai-Fu Chung (鍾采甫), Bo-Ming Huang (黃柏銘), and Jer-Ren Yang (楊哲人) Department of Materials Science and Engineering, National Taiwan University, Taipei, Taiwan	17
A-03	**Tempering Effect on Hydrogen Embrittlement of PA500H Steel** R.W. Liu[1](劉仁偉) W.H. Chien[1](簡文昊) H.W. Yen[1](顏鴻威) Y.T. Wang[2](王元聰) C.Y. Huang[2](黃慶淵) H.C. Lin[1*](林新智) [1]Department of Materials Science and Engineering, National Taiwan University, Taipei [2]Chinese Steel Company, Kaohsiung	19
A-04	**Characterization of homoepitaxial diamond film on Ni-coated (111) HPHT substrate** Kun-An Chiu（丘坤安), Jr-Sheng Tian（田志盛), Wei-Lin Wang（王尉霖), Lin-Lung Wei（魏伶容), Yue-Han Wu（吳岳翰), Chun-Yen Peng（彭峻彥), and Li Chang（張立）* Department of Materials Science and Engineering, National Chiao Tung University, Taiwan	21

Abstract-01

Conversion of ZnS into $Cu_{2-x}S$ superlattice in one-dimensional nanostructure through cation exchange reactions

[1]Chi-Lin Tsai(蔡季霖) and [1]Chuan-Pu Liu(劉全璞)

[1]Department of Materials Science and Engineering, National Cheng Kung University, Tainan 70101, Taiwan

*cpliu@mail.ncku.edu.tw

Copper sulfide is known to be an important p-type semiconductor. It exists in different phases ranging from copper-rich (Cu_2S) to sulfur-rich (CuS). Owing to the wide variation in their optical as well as electrical properties, copper sulfides find promising applications in various fields[1].

In this study, a two-step synthesis with chemical vapor deposition is employed. ZnS nanobelts were first synthesized using ZnS powders as the source, followed by the growth of $Cu_{2-x}S$ nanobelts through cation exchange reactions using $CuCl_2$ as the source [2]. The purpose of this study is to investigate the mechanism of cation exchange reactions through microstucture characterization of copper sulfide under different conditions in the second step. Fig.1 shows transmission electron microscopy (TEM) analysis of a typical porous $Cu_{1.8}S$ nanobelt after cation exchange reactions at 300℃ for 15 minutes, where superlattices and twins can be found. We will bulid up the atomic model of $Cu_{2-x}S$ superlattice structure.

References

1. Roy, P. and S.K. Srivastava, CrystEngComm, 17, 41 (2015)
2. Kim, Han Sung; Sung, Tae Kwang; Jang, So Young; Myung, Yoon; Cho, Yong Jae; Lee, Chi-Woo; Park, Jeunghee; Ahn, Jae-Pyoung; Kim, Jin-Gyu; Kim, Youn-joong: CrystEngComm, 13, 6 (2011)

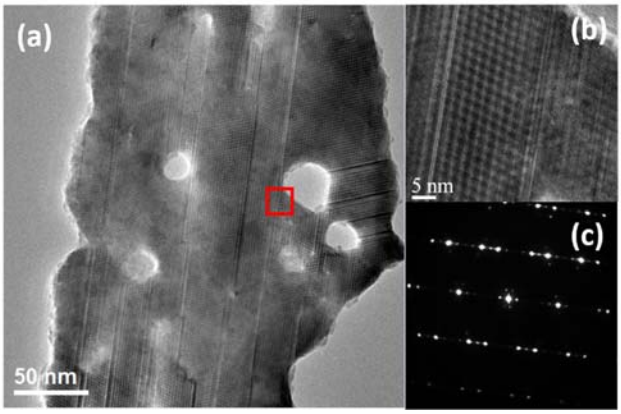

Figure 1. A $Cu_{1.8}S$ nanobelt by cation exchange reactions at 300℃ for 15 min. (a) TEM image (b) HRTEM from the red square region in (a) (c) diffraction pattern of (b)

Abstract-02

In-situ HRTEM investigation of the separated nucleation in the AA7050 aluminium alloy

Tsai-Fu Chung (鍾采甫)[1], Bo-Ming Huang (黃柏銘)[1], and Jer-Ren Yang (楊哲人)[1]

[1]Department of Materials Science and Engineering, National Taiwan University, Taipei, Taiwan

In this study, the investigation of the nucleation mechanisms has been investigated. The detail microstructure of precipitates such as GP zones, η' and η precipitates with their related orientation relationships respect to the Al matrix were explored by high resolution transmission electron microscopy (HRTEM). The precise transformation mechanism, such as GP zones→ η', has not been elucidated. In alloy steels, the transition of carbides has been explored in previous work [1] such as the separated nucleation and in-situ nucleation. Although a previous work [2] presumed that these two nucleation mechanisms occur during the transition of GP zones to η' phases, no direct evidence has been provided. The present study aimed to employ a series of in-situ HRTEM with low does electron beam to elucidate the related transition mechanisms.

Reference

[1] J. Yang, C. Huang, C. Yang, J. Horng, Mater. Charact. 30(2) (1993) 75-88.
[2] H. Löffler, I. Kovács, J. Lendvai, J. Mater. Sci. 18(8) (1983) 2215-2240.

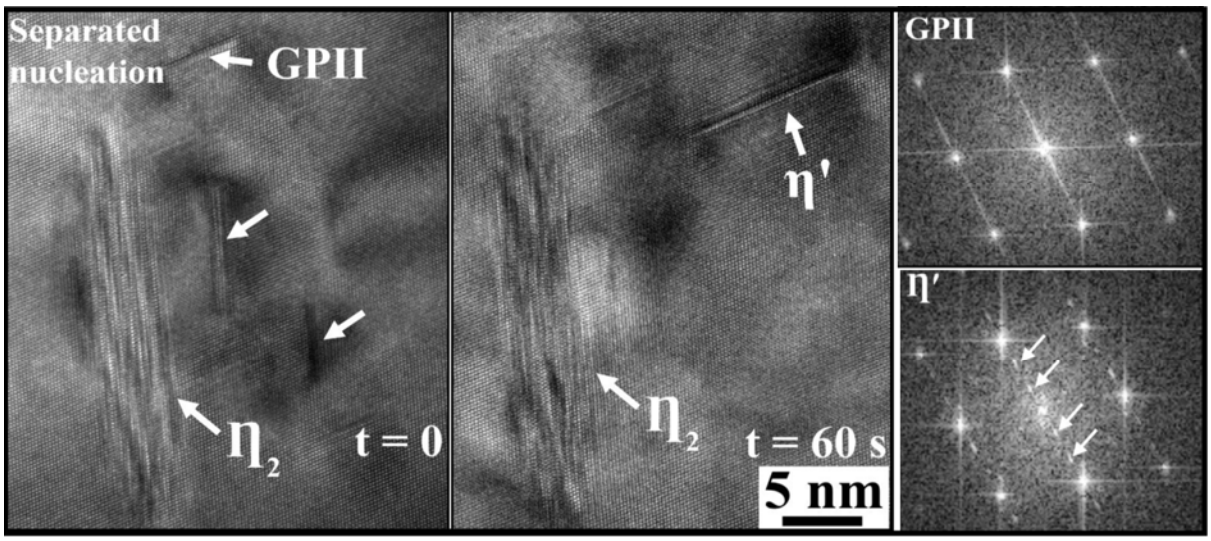
Separated
nucleation
GPII
η'
η2
t = 0
η2
t = 60 s
5 nm
GPII
η'

Abstract-03

Tempering Effect on Hydrogen Embrittlement of PA500H Steel

J.W. Liu[1](劉仁偉) Y.T. Hsu[1](徐宇彤) H.W. Yen[1](顏鴻威) Delphic Chen[2](陳志慶)
C.Y. Huang[2](黃慶淵) H.C. Lin[1*](林新智)

[1]Department of Materials Science and Engineering, National Taiwan University, Taipei
[2]China Steel Company, Kaohsiung
[*]hclinntu@ntu.edu.tw

PA500H steel is a high class wear-resistant steel. It is widely used in excavator and dump truck. It has a high yield strength, which is up to 1250 MPa. And it has a martensitic structure after direct quench. Martensitic type steels with this high strength level are very sensitive to hydrogen embrittlement. Therefore, the understanding of hydrogen embrittlement phenomena of PA500H is necessary. In this study, we investigate the hydrogen embrittlement of PA500H in various heat treatment conditions. We find that 180 ℃ tempering after direct quench can improve hydrogen embrittlement resistance. But higher tempering temperature such as 300℃ and 400℃ has a undesirable effect on improving hydrogen embrittlement resistance. After 180 ℃ tempering, fine ε-carbides precipitate inside martensite laths. These ε-carbides trap hydrogens and enhance the hydrogen embrittlement resistance. After 300℃ and 400℃ tempering, cementites are form between martensite laths. These cementites gather hydrogens to the martensite lath boundaries which reduce the hydrogen embrittlement resistance.

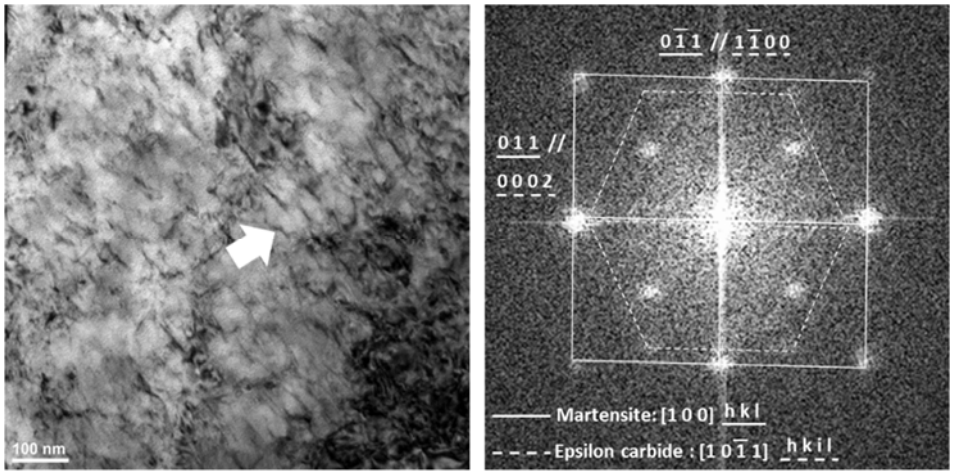

Figure 1. Fine ε-carbides precipitated inside the martensite laths, the bright field image and diffractogram.

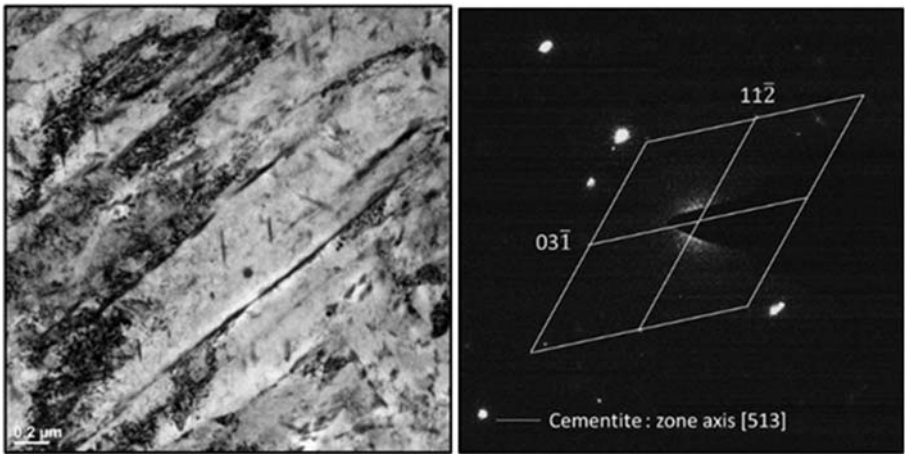

Figure 2. Cementite precipitated between the martensite laths, the bright field image and diffraction pattern.

References

1. S. Lynch, Hydrogen embrittlement phenomena and mechanisms, Corros Rev, 30 105-123 (2012).
2. S.M. Myers, Hydrogen interactions with defects in crystalline solids, Reviews of Modern Physics, Vol. 64, No.2 (1992).

Abstract-04

Characterization of homoepitaxial diamond film on Ni-coated (111) HPHT substrate

Kun-An Chiu（丘坤安), Jr-Sheng Tian（田志盛), Wei-Lin Wang（王尉霖), Lin-Lung Wei（魏伶容), Yue-Han Wu（吳岳翰), Chun-Yen Peng（彭峻彥), and Li Chang（張立）*

Department of Materials Science and Engineering, National Chiao Tung University, Taiwan
* lichang@nctu.edu.tw

Chemical vapor deposition (CVD) of homoepitaxial diamond film has been intensively studied for the last two decades. However, homoepitaxial growth of (111) diamond film by CVD which may be desired for n-type doping is more difficult than that of (100) because of mass formation of defects [1]. The (111) homoepitaxial diamond film tends to crack spontaneously by internal stress due to the presence of defects, non-diamond phases and impurities [2]. Recently the 5 μm-thick crack-free (111) homoepitaxial diamond film was successfully grown on Ni-coated high-pressure high-temperature (HPHT) substrate as a result of the stress reduction in CVD diamond with Ni islands [3]. Here we report the growth mechanism and dislocation analyses of the CVD diamond film on Ni-coated HPHT substrate.

The crack-free (111) homoepitaxial diamond film was grown on Ni-coated HPHT substrate by using microwave plasma enhance CVD. After hydrogen plasma annealing of the as-deposited Ni on the HPHT diamond substrate by using e-gun evaporation, single-crystalline and faceted Ni islands were heteroepitaxially formed with an orientation relationship of {111}Ni // {111}Dia and <110>Ni // <110>Dia. Cross-sectional TEM image shows that the (111) CVD homoepitaxial diamond film can be laterally overgrown across the Ni islands such as shown in figure 1. As measured with x-ray diffraction, the internal stress in the CVD diamond film on Ni-coated substrate can be significantly reduced with the nickel islands in comparison with those in the film directly grown on HPHT substrate. The dislocation density in the CVD diamond film on Ni-coated substrate is approximately 4.5×10^8 cm^{-2}. The types of dislocations were composed of screw dislocations and 60° mixed dislocations.

References

1. N. Casanova, A. Tajani, E. Gheeraert, E. Bustarret, J.A. Garrido, C.E. Nebel, M. Stutzmann, Diam. Relat. Mater., **11** 328 (2002).
2. Mermoux M, Marcus B, Crisci A, Tajani A, Gheeraert E, Bustarret, Diam. Relat. Mater., **13** 329 (2004).
3. K.A Chiu, J.S. Tian, Y.H Wu, C.Y. Peng, L. Chang, Surf. Coat. Technol., **259** 358 (2014).

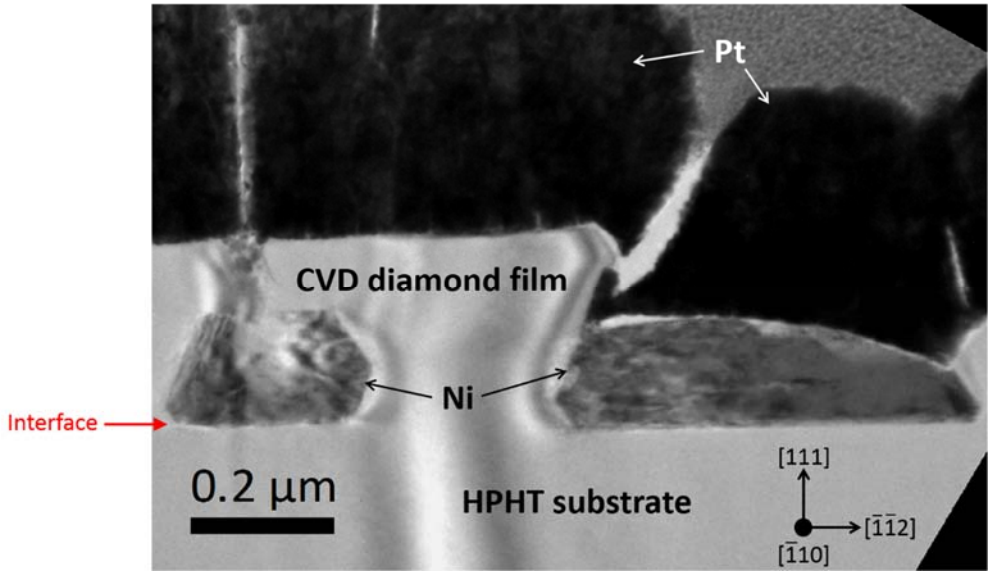

Figure 1. Bright field cross-sectional TEM image of ~ 300 nm thick diamond grown on Ni-coated substrate. TEM specimen was prepared by focused ion beam with Pt coating.

Abstract-05

Influence of Austempering Temperature on Morphology and Stability of Retained Austenite in Interphase Precipitation Strengthened Multi-phase TRIP Steels

Shih-Ning Tsai（蔡世寧）[1*], Shao-Pu Tsai(蔡劭璞)[1], and Jer-Ren Yang（楊哲人）[1]

[1]Department of Materials Science and Engineering, National Taiwan University, Taipei, Taiwan

[*]r04527011@ntu.edu.tw

Through TEM observation, nanometer-sized interphase-precipitated carbides indeed disperse densely in ferrite phase. Utilizing EBSD, XRD, TEM and CBED techniques, experimental results show that austempering temperature influence the amount of bainite formation, resulting in different microstructure morphology in second phase island with different quantity and carbon content of retained austenite. It is found that there are three different types of morphology of retained austenite: Type I: Thin film austenite between bainite sub-units； Type II: Large film austenite between bainite sheaves； Type III: Blocky austenite in second phase island adjacent to ferrite grain boundary. Austenite dimension: Type III > Type II > Type I. Carbon content and stability of austenite: Type I > Type II > Type III. The amount of bainite formation decrease as the austempering temperature increase. Therefore, the fraction of large-sized retained austenite gradually increase. Also, the amount of large block M/A phase increase with increasing austempering temperature.

By tensile test, the specimen austempered at 390°C has the best ductility, instead of the specimen austempered at 420°C which has the highest retained austenite content. During deformation process, the austenite retained after austempering at 390°C gradually transform to martensite thanks to high carbon content and stability. The work hardening rate is kept high at large strain and contribute TRIP effect to improve elongation. Although the specimen austempered at 420°C has the highest retained austenite content, the carbon content and stability of retained austenite is low. Consequently, most retained austenite rapidly transform to martensite at early stage of deformation process. At large strain, the work hardening rate is unable to be kept high and no more TRIP effect can be generated, leading to lower elongation.

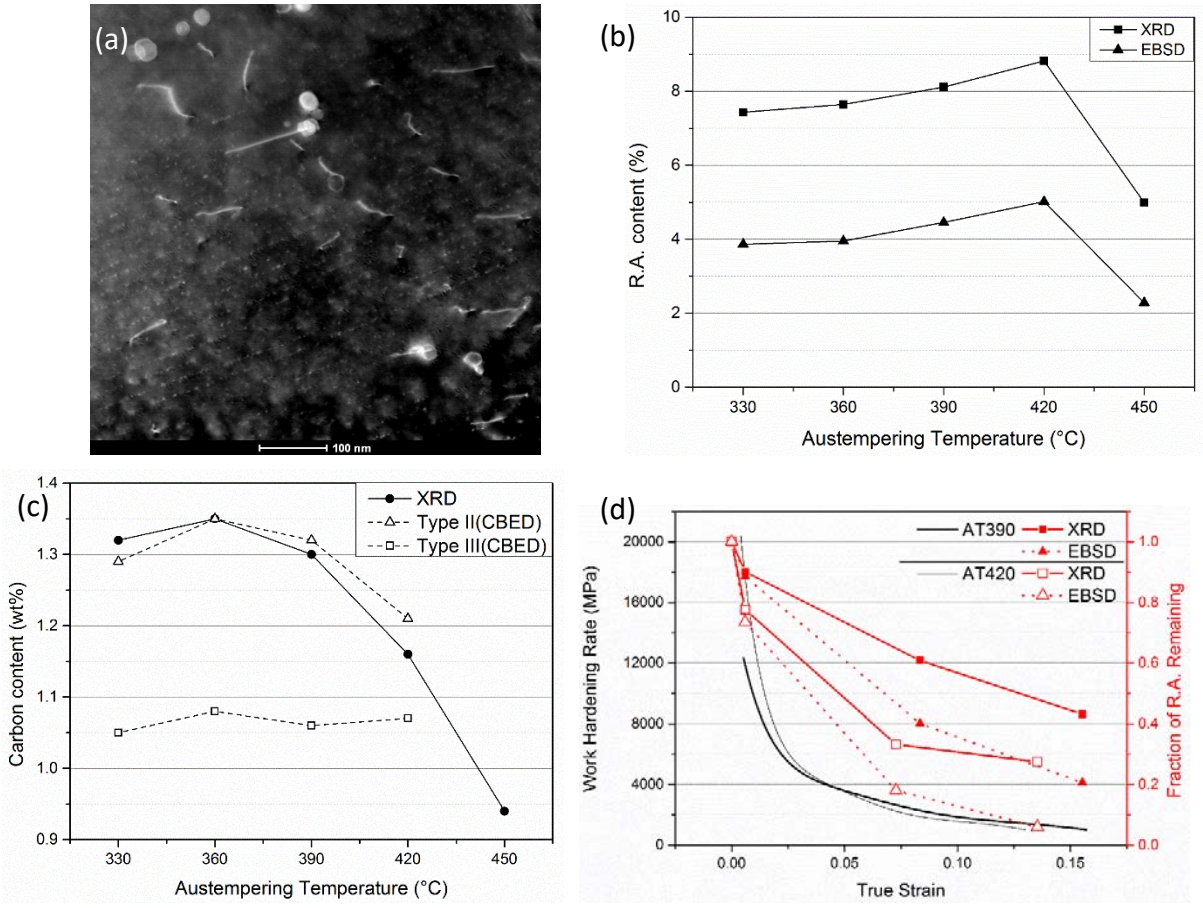

Figure 1. (a)TEM micrograph of interphase-precipitated carbides, (b)R.A. content and(c)carbon content in R.A. with different austempering temperature, (d)R.A. content during deformation.

Abstract-06

Warm Ductility Enhanced by Austenite Reversion in Ultrafine-Grained Duplex Steel

Guan-Ju Cheng (程冠儒),[1] and Hung-Wei Yen (顏鴻威)[1*]

[1]Department of Materials Science and Engineering, National Taiwan University, Taipei, Taiwan

[*]homeryen@ntu.edu.tw

The current work investigated the relationship between microstructure and warm deformation properties in a strong but ductile Mn-rich steel. A cold-rolled Fe-11Mn-0.068C (in wt.%) steel was deformed isothermally after inter-critical annealing at 550°C to 720°C. It was found that deformation at 600°C and 650°C leads to a high ductility (total elongation over 90 %) because phase transformation accompanied with deformation. The microstructure was characterized by transmission kikuchi diffraction (TKD). Austenite were only elongated at severe deformed region (area reduction is about 50%) with strain rate 0.001/s. This research could provide metallurgical information in designing strong but ductile steels for hot processing.

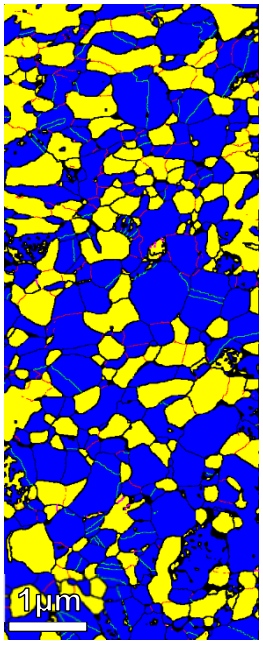

Figure 1. Transmission kikuchi diffraction mapping of the Mn-rich steel after inter-critical annealing at 650 ºC for 10 min

Abstract-07

Investigation of Using Diversed Metal/Alloy Catalysts to Grow the GaN Nanowires by Hydride Vapor Phase Epitaxy

Wei-Cheng Yu (游瑋丞)*, Fang-Yi Lin (林芳宜), Chih-Chaing Yang (楊智強), Wei-I Lee (李威儀), and Yi-Chia Chou (周苡嘉)

Department of Electrophysics, National Chiao Tung University, Hsinchu, Taiwan

* presenting author: Wei-Cheng Yu, email:wayne123017@gmail.com

Gallium nitride (GaN), with wide direct bandgap of 3.4 eV as semiconductor, plays a crucial role in current optoelectronics and high-power electronics [1]. As the scale of devices becomes smaller, low-dimensional GaN nanowires (NWs), a new class of advanced materials, have attracted considerable research interest because of their particular physical properties and potential applicability as building blocks in the development of novel nanodevices [2].

In recent years, GaN NWs have been synthesized with the vapor-liquid-solid (VLS) or vapor-solid-solid (VSS) mechanism, which makes use of foreign catalyst elements for the nucleation and growth of NWs [3]. Here, we report GaN NWs grown on Si (111) substrate through hydride vapor phase epitaxy using Au, Au/Ni and Au/Mn as catalysts. Metals were deposited on the substrate by e-gun evaporator. We use transmission electron microscopy (TEM) to study the GaN NWs microstructure from various metal/alloy catalysts. The growth mechanism and catalyst/NW epitaxy will be discussed.

References

1. S. Nakamura. "Nobel Lecture: Background story of the invention of efficient blue InGaN light emitting diodes." Review of Modern Physics, 87, 1139, 2015.
2. W. Molnar et al. “Subeutectic synthesis of epitaxial Si-NWs with diverse catalysts using a novel Si precursor.” Nano Lett. 10, 3957–3961, 2010.
3. G. Avit et al. “Ultralong and defect-free GaN nanowires grown by the HVPE process.” Nano Lett. 14, 559−562, 2014.

Abstract-08

Study of Self-Propagating Reaction in the Ni/amorphous-Si Reactive Multilayers

Wen-Hsien Hsu(徐文賢)[1], Chien Chang (張阡)[1], Yi Chou (周易)[1],
Yi-Chia Chou (周苡嘉)[1]

[1] Department of Electrophysics, National Chiao Tung University, Hsinchu City, Taiwan

Reactive multilayers are composed of nanoscale interlaced materials. By a localized heating treatment, a portion of multilayers intermixes and releases latent heat of reaction, which further mixes the adjacent region and generates gasless self-propagating flame [1]. The reaction features localized high reaction temperature (up to 1000K-3000K) [2], small total amount of heat release and unusual high propagating rate (up to tens of meters per second), which enables the reactive multilayers to be used in applications such as jointing materials and initiator to produce optical signal and reaction initiator [3].

For this study, the properties of self-propagating reaction in the Ni/α-Si systems such as surface modulation, speed of propagation, morphology of reaction product and reaction mechanisms will be discussed. In our experiment, we found that the steady state of self-propagating reaction is critical to produce the flat and uniform product surface.

References

1. K. Woll et al. Scientific Reports **6**, 19535(2016)
2. D. P. Adams et al. Thin Solid Films **576**, 98(2015)
3. T. P. Weihs, Metallic films for electronic, optical and magnetic applications - Structure, processing and properties. Woodhead, Cambridge, UK (2014).

Abstract-09

Coopetitive relationships and micro-mechanisms of recrystallization and transformation during/after dynamic strain-induced transformation in Al-containing low-carbon steel

Shih-Che Chen (陳世哲)[1], Cheng-Yao Huang (黃正堯)[1], Yuan-Tsung Wang (王元聰)[2] and Hung-Wei Yen (顏鴻威)[1*]

[1]Department of Materials Science and Engineering, National Taiwan University, Taipei, Taiwan

[2]Iron and Steel R&D Department, China Steel Corporation, Chung Kang Road, Kaohsiung, Republic of China

[*]homeryen@ntu.edu.tw

In this work, the coopetitive relationships among dynamic strain-induced ferrite transformation, reverse transformation and austenite recrystallization were investigated by using dynamic dilatometry, optical metallography and electron backscattering diffraction in Al-containing low carbon steel after/during hot compressions in the two-phase region. The microscopic mechanisms of concurrent and successional dynamic softening were studied based on the analysis of transformation crystallography. It was demonstrated that the occurrence of reverse transformation leads to the formation of new austenite grains, which can act as nucleation site and further induce austenite recrystallization. These paths for microstructural control in steels are not common, but they can be enabled by critical thermo-mechanical treatments combined with proper alloy design.

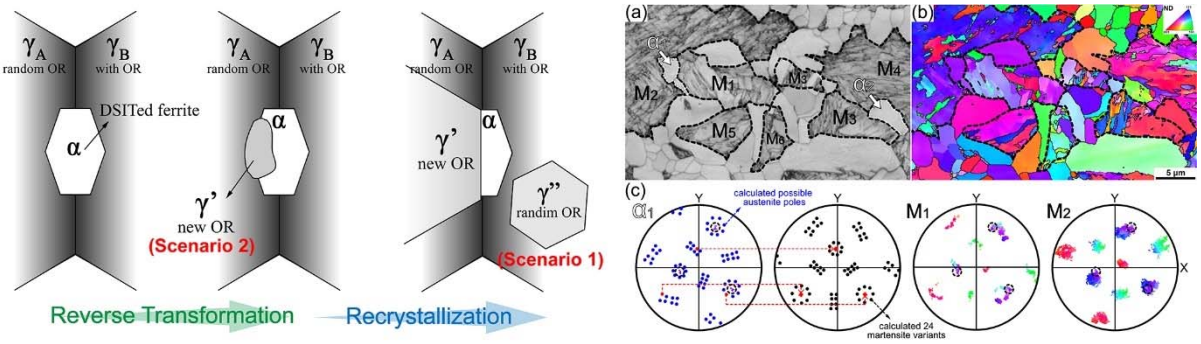

Figure 1. Schematic illustration (left) and electron backscattering diffraction analysis (right) represent the micro-mechanism of reverse-transformation-induced recrystallization after dynamic strain-induced transformation.

Abstract-10

A New Method of Phase Quantification in Complex Steels by EBSD

Yu Wen Chen (陳昱文), Tung Po Yen (童博彥), Yu Ting Tsai (蔡宇庭)[1] and Jer-Ren Yang (楊哲人)[1*]

[1]Department of Materials Science and Engineering, National Taiwan University, Taipei, Taiwan

[*]jryang@ntu.edu.tw

A new method for microstructure and phase quantification in complex-phase low carbon Nb-Mo bearing steels is developed. In the previous studies, large amount of polygonal BCC structures and degenerated pearlite are found in the low carbon steels with medium cooling rate. In the optical metallography, the granular shape ferrite grains are almost identical and cannot be discriminated in the BCC matrix. However, it is possible to differentiate the microstructures in the TEM observation, and there are two totally different sub-structure in the granular-shaped ferrite. The lath structure with 500 nm width in the low carbon steels named granular bainite. Although TEM can be used to distinguish microstructures, its capability for phase quantification is limited owing to small observation area. EBSD combined with kernel average misorientation (KAM) can be used for phase quantification. In this study, the KAM mapping with different kernel size and various step size are investigated. It is concluded that the kernel size close to the sub-structure size is the optimal condition for phase quantification. With appropriate kernel size and large step size, phase quantification by EBSD mapping can save much time without compromising accuracy.

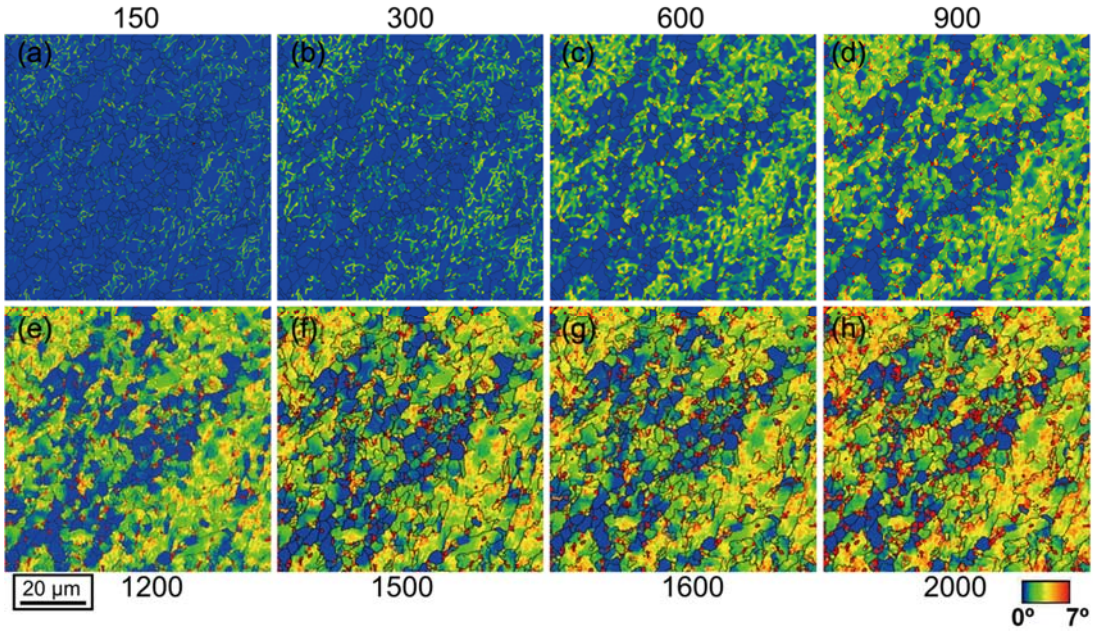

Figure 1. The KAM mapping versus various kernel size in low carbon Nb-Mo steels.

Abstract-11

Effects of low-temperature asuforming on the miscrostructural evolution in Fe-0.6C-2Si-2Mn nanobainitic steels

Po-Yen Tung (童博彥)[1], Yu-Ting Tsai (蔡宇庭)[1], and Jer-Ren Yang (楊哲人)[1*]

[1]Department of Materials Science and Engineering, National Taiwan University, Taipei, Taiwan

[*]jryang@ntu.edu.tw

Nanostructured bainite [1], having high potential as the bulletproofing material, has been studied for many years. Nanostructured bainite possesses high strength, high elongation, but its low toughness due to the instability of blocky austenite is a serious disadvantage. So, the primary propose in this work is to improve the properties of blocky austenite. First, we introduce ausforming process—plastic deformation at low temperature before isothermal bainitic transformaiton—to change the microstructure of traditional nanostructured bainite. Second, we further measure the stability of blocky austenite in ausformed bainite by EBSD. Besides, the orientation relationship between blocky austenite and bainitic ferrite is analyzed by EBSD. In ausformed bainite, the blocky austenite and bainitic sheaves are simultaneously refined and well-distributed. The refined blocky austenite is further mechanical stabilized by ausforming process, which might benefit to mechanical properties. Due to ausforming process, variant selection is assisted by Shockley partial dislocations and measured by EBSD.

References

1. F.G. Caballero, H. Bhadeshia, K.J.A. Mawella, D.G. Jones, P. Brown, Mater. Sci. Technol., 18 (2002) 279-284.

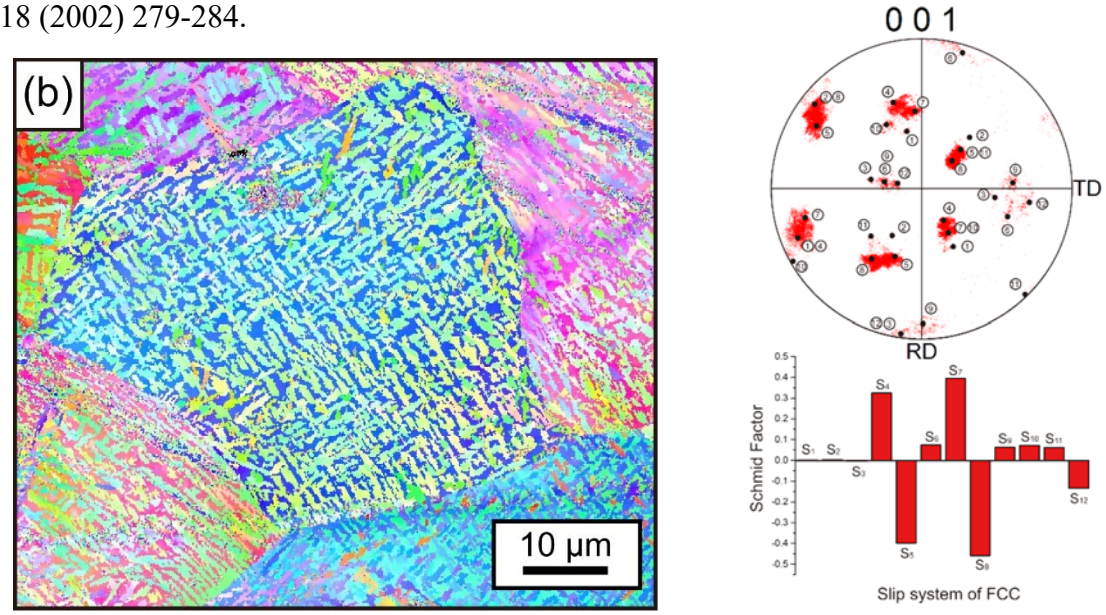

Figure 1. Inverse pole figure (IPF) map of ausformed specimen with bainitite variant selection. The relationship between slip systems and crystallography of bainitic ferrite.

Abstract-12

Particle Size Analysis of the $CsPbX_3$ Nanocrystals

Ren-Fong Cai (蔡任豐),[1*] Sheng-Min Yu (游勝閔),[1] and Shen-Chuan Lo (羅聖全)[1]

[1]Department of Materials Science and Engineering, National Taiwan University, Taipei, Taiwan

[*]renfong@itri.org.tw

$CsPbX_3$ (X=Cl, Br and I or mixed halide system) nanocrystal is one of the promising optoelectronic materials. The size of $CsPbX_3$ crystal is the key factor for cubic phase stabilization in room temperature [1]. In order to estimate the size of $CsPbX_3$ precisely, we used the computer program for measuring large amount of the particles. However the brightness of the particles are varied drastically due to the diffractive contrast, it is very difficult to separate the particle object from the background. In this study, we applied contrast limited adaptive histogram equalization (CLAHE) filter to enhance the contrast from particle to background [2].The result as shown in figure1, and the filtered image gives the better result than the raw image. We analyzed 2,017 particles from 7 images and the average equivalent diameter is 17.04 nm.

References

1. A. Swarnkar et. Al., Science, **6308** 354 (2016).
2. K. Zuiderveld, Graphics Gems IV, Academic Press (1994).

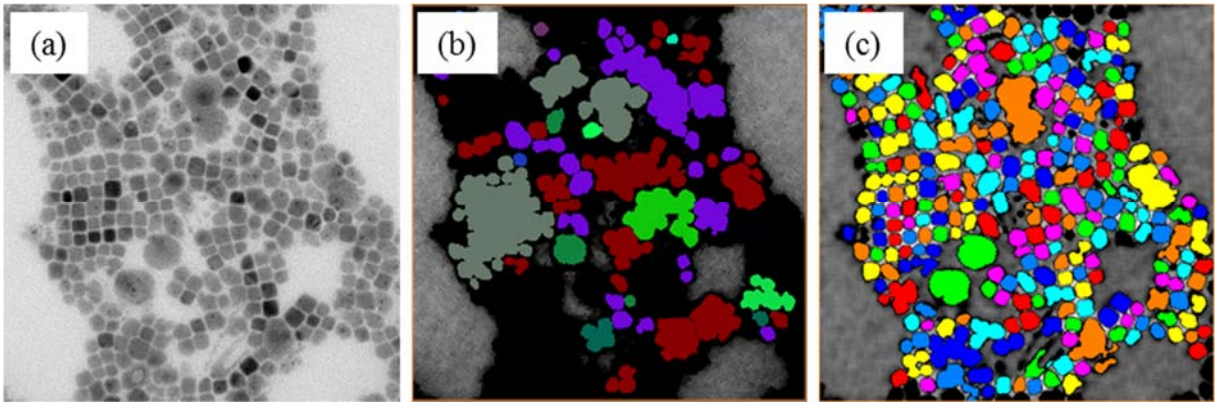

Figure 1. (a) Raw image. (b) Particle size analysis of the raw image. (c) Particle size analysis of the CLAHE filtered image.

Abstract-13

Effect of isothermal holding temperatures on microstructure and mechanical properties of interphase precipitation strengthened dual-phase steels in a low C Ti-V-bearing steel

Shao-Pu Tsai（蔡劭璞）[1*], Yuan-Tsung Wang（王元聰）[2], Chin-Yuan Huang（黃慶淵）[2], and Jer-Ren Yang（楊哲人）[1]

[1]Department of Materials Science and Engineering, National Taiwan University, Taipei, Taiwan

[2]Department of Research and Development, CSC, Kaohsiung, Taiwan

[*]f01527016@ntu.edu.tw

Low carbon Ti and Ti-Mo bearing steels were investigated in the present study. Different isothermal holding temperatures of 650°C, 680°C, 700°C, and 720°C were applied to generate different dual-phase morphology with interphase precipitation inside ferrite. Holding time was especially controlled for the similar volume percent of martensite. Grain size of dual-phase structures decreases with decreasing holding temperatures for both steels. It is found that ferrite hardness increases with decreasing holding temperatures; martensite hardness is on the inverse trend. Ti and Mo together make a higher ferrite hardness yet lower martensite hardness. Carbon content in martensite is used to explain the hardness variation in martensite. For lower holding temperature, the dual-phase structure has higher strength together with larger elongation both for Ti and Ti-Mo-bearing steels. Higher ferrite strength, lower ferrite/martensite hardness difference, and reduced dual-phase size are used to explain the mechanical behaviors. Careful TEM observation confirmed the existence of interphase precipitation, whose sheet spacing and intercarbide spacing decrease with decreasing temperature, and enormously increase strength contribution (see Figure 1). Martensite morphology was also observed to be different, which accords with the hardness variation.

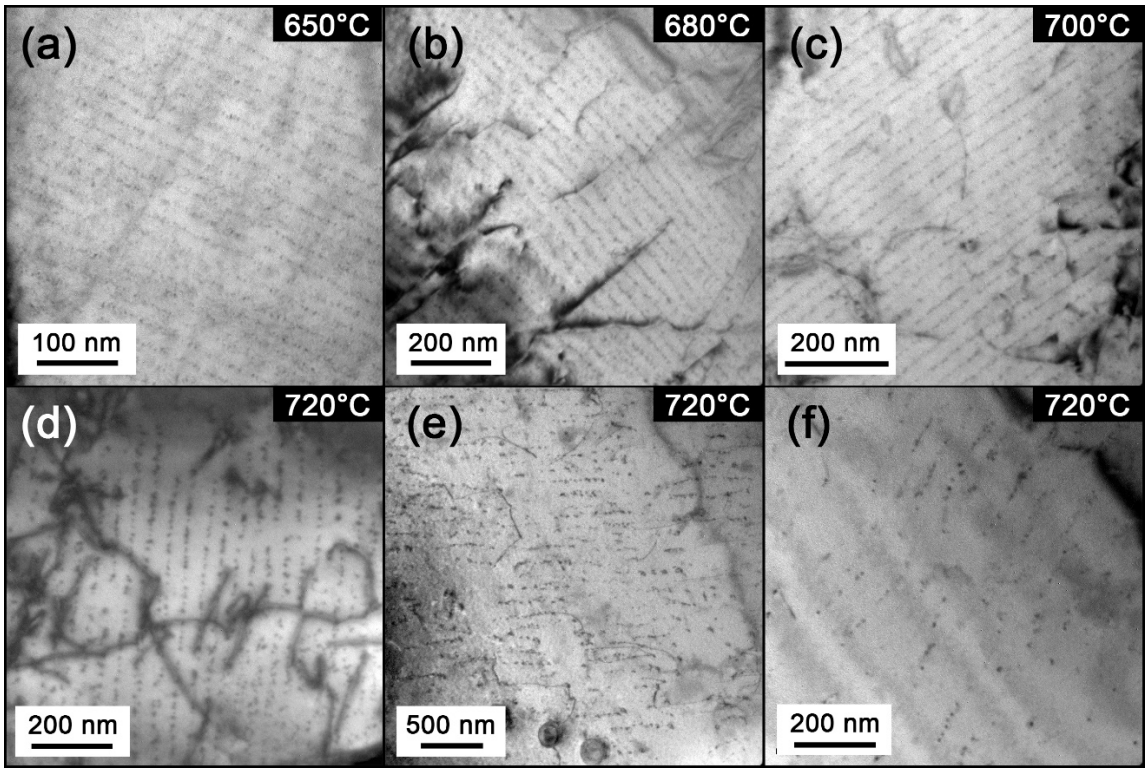

Figure 1. Interphase precipitation found in Ti-bearing samples held at different holding conditions: (a-c) 650°C, 680°C, 700°C; (d-f) 720°C.

Abstract-14

The Weldability of High Strength Offshore Steels - Microstructure Analysis

Sz-Yuan Hu（胡思源）[1], and Mei-Jing Lin（林美均）[1], and Cheng-Yao Huang（黃正堯）[1], and Hsin-Chih Lin (林新智) [1*], and Hung-Wei Yen（顏鴻威）[1*],

[1]Department of Materials Science and Engineering, National Taiwan University, Taipei, Taiwan

*hclinntu@ntu.edu.tw *homeryen@ntu.edu.tw

Abstract:

This research is focused on developing the S690Q high strength steels by TMCP+DQ+T processing to investigate weldability. The investigation includes related mechanical properties test and microstructure analysis of heat affected zone (HAZ) simulation. Different welding parameters are tested and provided for submerged arc welding. The microstructure evolution can show the relationship between thermal cycles and their mechanical properties. Compared to real single-pass weldment, the same microstructures can be observed in HAZ simulation. Results above are applied to optimize related processes, and provide a total solution of S690Q steel for large-scaled offshore wind turbine application.

Abstract-15

Orientation Relationship of TiN with Nitrided Rutile (001) Substrate

Ching Chang（張敬）, Lin-Lung Wei (魏伶容), Kun-An Chiu（丘坤安）, and Li Chang（張立）*

Department of Materials Science and Engineering, National Chiao Tung University, Hsinchu, Taiwan

*lichang@nctu.edu.tw

One of conventional synthesis techniques for TiN has been nitridation of titania (TiO_2), usually in the form of particles. Nitridation of single crystalline titania may be helpful for understanding the fundamental mechanism for nitride formation without much complicated effects from microstructural defects. Here, we report the orientation relationship of TiN formed on nitrided rutile (001) substrate by nitrogen plasma. Figure 1 shows a typical cross-sectional STEM-ADF image in Z-contrast obtained from a region around the TiN/TiO_2 interface. From the FFT patterns, TiO_2 in <110> zone axis (rutile in tetragonal structure) can be recognized, whereas TiN is in <001> one, indicating <110> TiO_2 // <100>TiN. Furthermore, TiO_2 (001) is parallel to TiN (011). From the newly found orientation relationship, it is understood that nitridation of rutile may proceed along [001] to form oriented TiN in <110>.

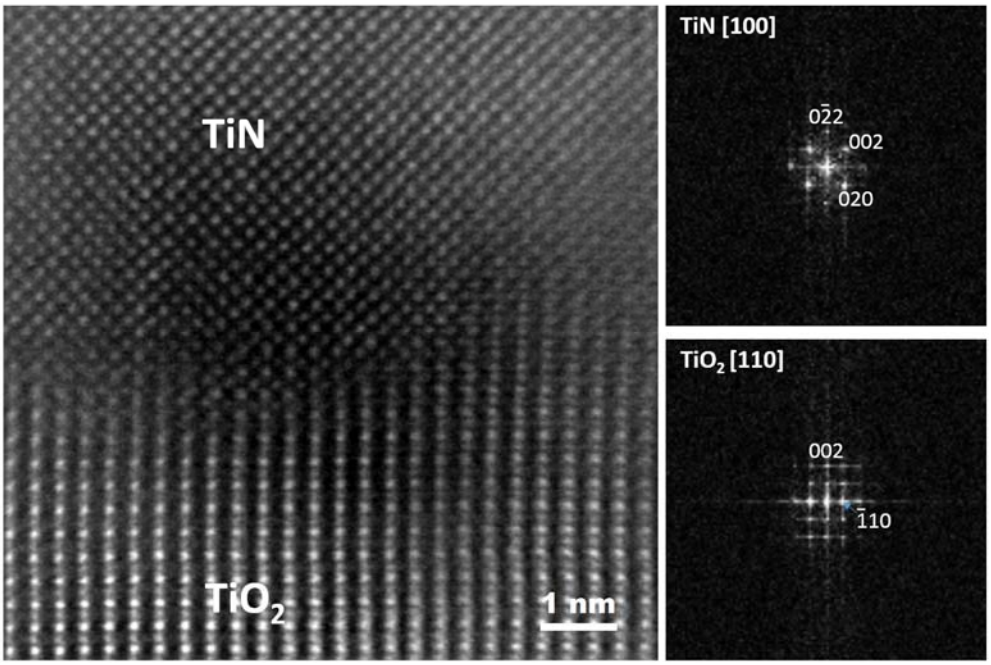

Figure 1. STEM-ADF image obtained from TiN/TiO_2 interface with FFT patterns of TiN and TiO_2.

Abstract-16

Atomic Layer Deposition of Aluminum-doped TiO_2 Thin Films

I-Ta Wang (汪奕達)[1*], Chien-Ting Wu (吳建霆)[2] and Cheng-Yen Wen (溫政彥)[1]
[1]Department of Materials Science and Engineering, National Taiwan University, Taipei, Taiwan
[2]National Nano Device Laboratories, Hsinchu, Taiwan
Email: *b02507005@ntu.edu.tw

TiO_2 has many advantages for future electronics and energy applications, such as earth-abundant, environmental friendly, resistance to corrosion, non-toxic to human, etc. [1]. However, the intrinsic TiO_2 is an n-type semiconductor due to oxygen deficiency in its structure. It will be advantageous if we can fabricate p-type TiO_2 to replace other p-type oxide semiconductor materials. In this study, we intend to dope aluminum in TiO_2 in order to prepare a p-type TiO_2 thin film. It is expected that by doing this we can also make a more efficient photocatalyst TiO_2 thin film or make a homogeneous p-n junction interface. The atomic layer deposition (ALD) process provides us a method to deposit thin film uniformly on any surface structure and precisely control the composition of thin films [2]. In order to make uniform aluminum distribution in TiO_2 thin films, we try two different methods, including interdiffusion in Al_2O_3/TiO_2 bilayer (Fig. 1(a)) and $TiO_2/Al_2O_3/TiO_2$ trilayer (Fig. 1(b)) structures and in-situ Al_2O_3/TiO_2 ALD growth (Fig. 1(c)). Transmission electron microscopy (TEM), Auger electron spectroscopy (AES), and electron dispersive spectroscopy (EDS) are used to analyze the deposited thin films. We find that the in-situ deposition process makes uniform aluminum distribution in TiO_2 thin films. The electrical properties of these thin films will be determined by the Hall measurement and the Seebeck coefficient measurement.

References

1. V.C. Anitha, A.N. Banerjee, and S.W. Joo, *Journal of Materials Science* **50**, 7495 (2015).
2. S.M. George, *Chemical Reviews* **110**, 111 (2010).

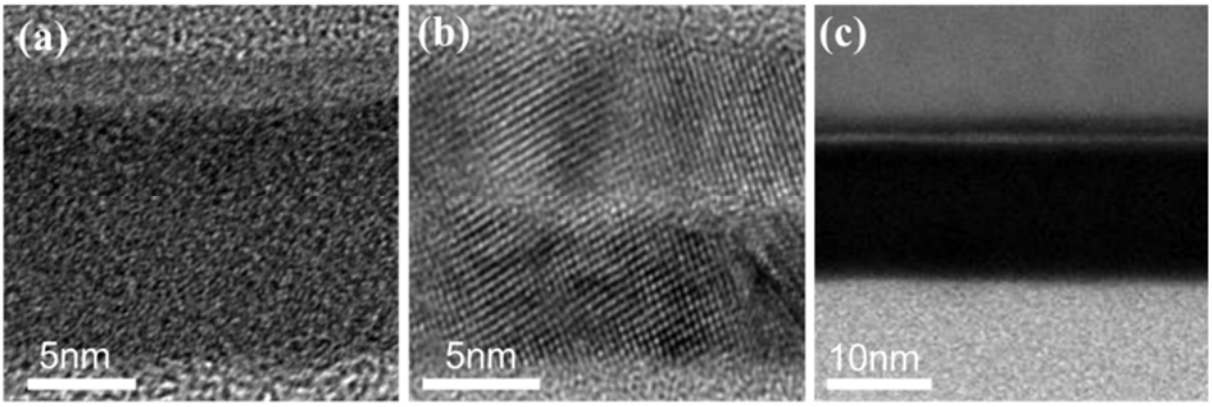

Figure 1. (a) TEM image of the Al_2O_3/TiO_2 bilayer structure. (b) TEM image of the $TiO_2/Al_2O_3/TiO_2$ trilayer structure. (c) Scanning TEM (STEM) image of the Al_2O_3/TiO_2 thin film by in-situ ALD growth.

Abstract-17

Visualization of Electron Channeling Pattern

Yu-Ting Tsai (蔡宇庭),[1] and Jer-Ren Yang (楊哲人)[1*]

[1]Department of Materials Science and Engineering, National Taiwan University, Taipei, Taiwan

[*]jryang@ntu.edu.tw

The physical principles for fascinating electron channeling pattern are not easily comprehensible, and most introductory materials provide associated image resembling Figure 1a. However it is not easy to understand the pattern origin other than formidable theoretical approach. To elucidate the understanding of electron channeling, in this work, the visualization of electron channeling pattern was conducted by computer-generated three dimensional grid. The associated pole figure of the three dimensional girds is plotted, and is shown in Figure 1b. For a simple cubic lattice, the projection of the grids resembles that obtained in electron channeling patterns. The reason for this similarity is that every black dot in the grids is blocking the white background, just like every atom in regular array is blocking the electron beams. Moreover, as illustrated in Figure 1b, low-index zone axes as well as low-index bands provide wider channels for electron to propagate through, thus generating higher signals.

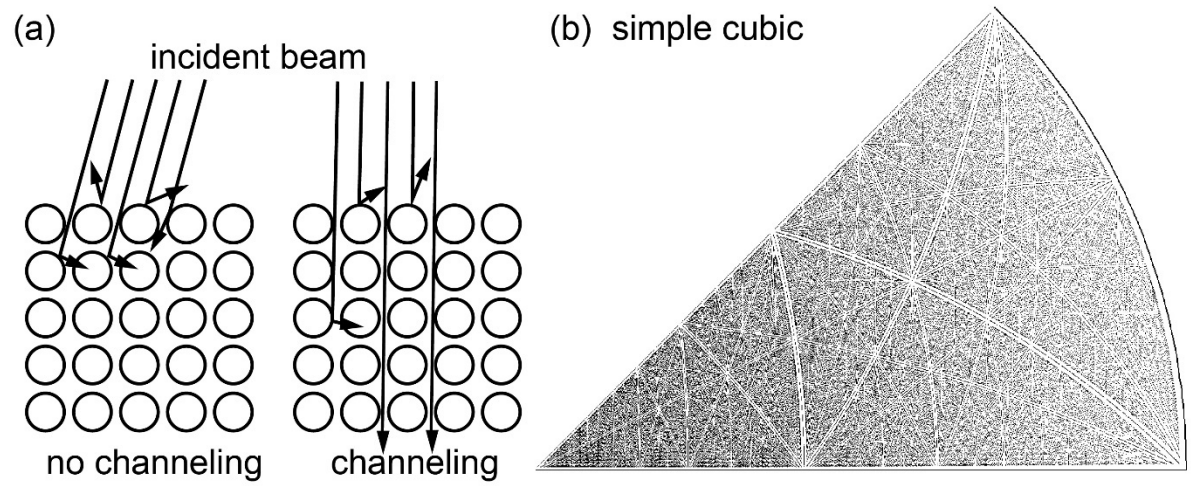

Figure 1. (a) illustration of channeling effect. (b) calculated pole figure for simple cubic grids.

[1] Coates DG, *Phil. Mag.* (1967), 16, 1179.

[2] D.C. Joy, D. E. Newbury, D. L. Davidson, *J. App. Lett.*, (1982), 53, R81.

Abstract-18

Microstructure characterization of atypical lenticular martensite in Fe-0.7C-13r stainless steel

Shih-Wen Lai (賴世雯),[1] and Jer-Ren Yang (楊哲人)[1*]

[1]Department of Materials Science and Engineering, National Taiwan University, Taipei, Taiwan

[*]jryang@ntu.edu.tw

The microstructure of atypical lenticular martensite in Fe-0.7C-13r stainless steel has been studied by EBSD, TKD, and TEM in this research. In Fe-0.7C-13r stainless steel, after austenization treatment at temperatures 1200°C for three days, austenite was stable at room temperature and would transform to lenticular martensite after subzero treatment. During analyzing of EBSD results of lenticular martensite, some peculiar microstructures of lenticular martensite were observed. Because of the large interaction volume and the limited resolution of EBSD, TKD and TEM were used to confirm that those microstructures were actual microstructure rather than misleading results due to EBSD limitations. In Fe-0.7C-13r stainless steel, those microstructures could be considered atypical lenticular martensite.

References

1. S. Suzuki, Jom, 65.9 1254 (2013)

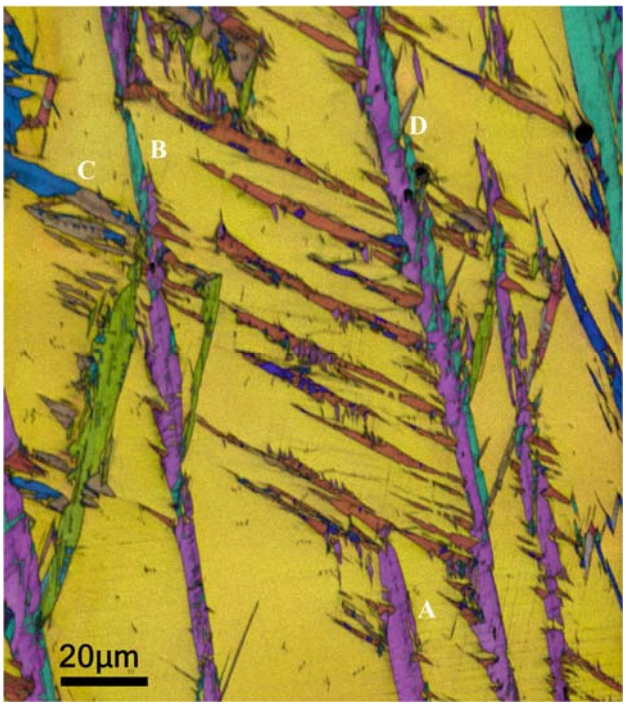

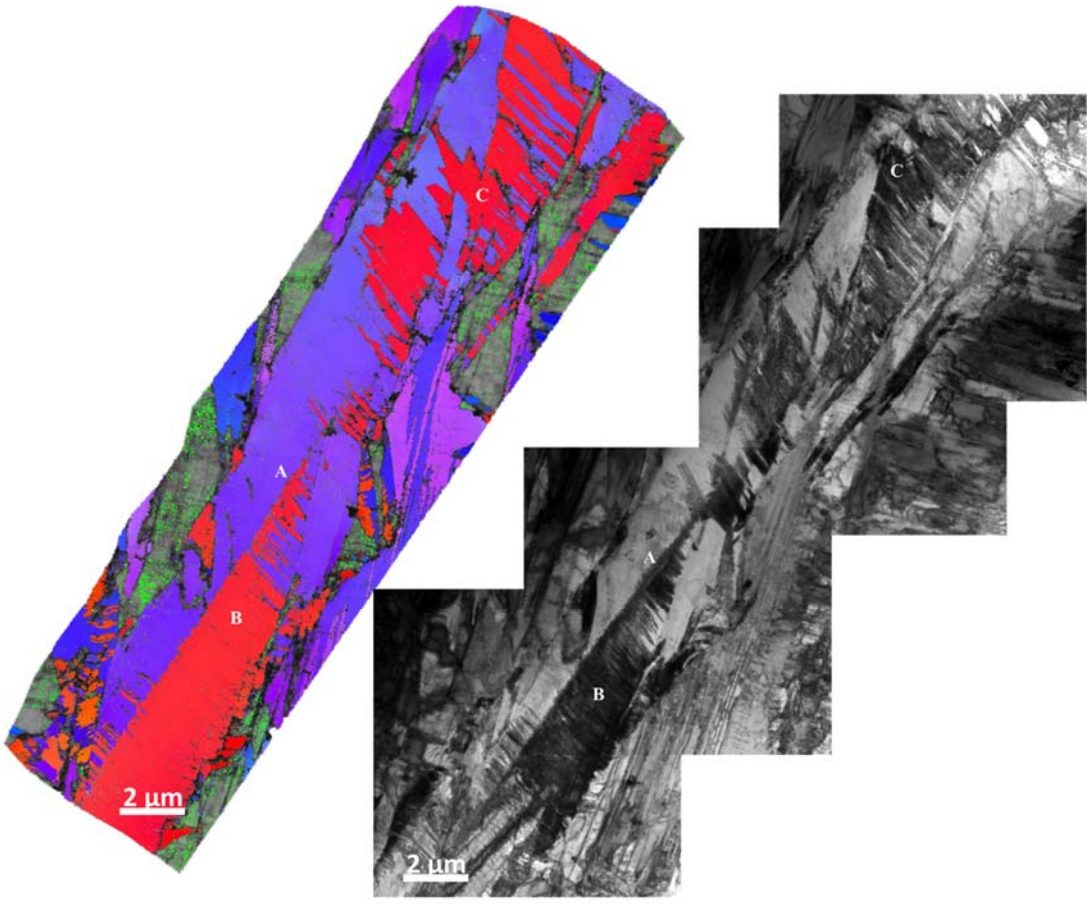

Figure 1. EBSD, TKD and TEM images of atypical lenticular martensite

Abstract-19

TEM Metrology Enabler - A New Calibration Methodology

Li-Heng Chen(陳利恆)*, Min-Nin Yu(余敏寧)
, Bi-Hui Lee(李碧惠) and Vincent D.-H. Hou (侯敦暉)

Taiwan Semiconductor Manufacturing Company, Limited, Transmission Electron Microscopy Department, Taiwan
*lhchenv@tsmc.com

There is a constant need to "shrink" Si transistors to meet our insatiable demands for smaller and more powerful devices. Consequently, TEM based metrology plays an ever increasing role in advanced process nodes (20nm and beyond). **Motivation:** Improve TEM metrology accuracy and minimize cross-tools deviation in an efficient way. **Challenges**: Can we 1) have a better calibration standard and methodology; and 2) improve calibration/tool matching efficiency? **Current Status**: The special MAG*I*CAL sample is a well-accepted TEM calibration standard but it exhibits ±2% uncertainty at the commonly used field-of-view range (100-300nm). In addition, the calibration procedure which requires measuring lattice spacing on HREM images is very inefficient. **Innovation:** 1) Use Si lattice spacing (Si d_{111} = 0.31355 nm[1], which can be routinely resolved in HREM images) as the calibration standard. It is easily attainable and virtually every TEM sample with Si substrate can be used as calibration standard; 2) Si lattice plan spacing is measured automatically with a software algorithm in reciprocal/FFT space [2,3]. **Major achievements:** 1) Calibration can now be derived from multiple measurements (i.e. averaged from >10 images), which is statistically relevant; 2) TEM tool matching accuracy improve significantly (GRR test)

References

3. [CRC Handbook of Chemistry and Physics, CRC Press, Inc., Boca Raton, Florida33431].
4. W.J. de Ruijter et al., Ultramicroscopy 57 (1995) 409-422
5. DM script implementation: http://donation.tugraz.at/dm/source_codes/140

Pattern vs Si lattice

As is

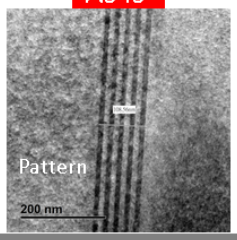

To be

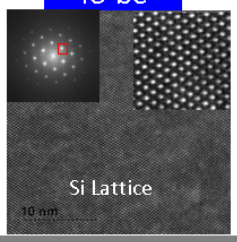

The R-squared~ 0.9756 from Si lattice and pattern CD correlation

Pattern	Item	Si Lattice
Pattern real ? unknow	Standard	**✓Si theoretical d-spacing (111)**
Weak → Sample amount: only one	Sample damage	✓Much better→ Sample amount: unlimited
(identical site)→Only one	Sample amount	✓Resource unlimited
Manual measure(%R&R: 57.99%→unacceptable)	Accuracy	✓Auto measure by algorithm (%R&R:1.82%→satisfactory)

Abstract-B-01

Trait differences between variegated and non-variegated forms of *Begonia formosana*, and correlations between leaf and reproductive characteristics

Yi-Sian Lin（林宜憲）[1], Peter Chesson[1,2] and Chiou-Rong Sheue（許秋容）[1]

[1]Department of Life Sciences, National Chung Hsing University, Taiwan;
[2]University of Arizona, USA

Natural foliar variegated plants are occasionally found in forest understoreys. *Begonia formosana*, a shade herb native to Taiwan, has two forms, variegated and non-variegated (green form). The mechanism of foliar variegation in *B. formosana* has been reported to be the air space type (structural variegation), with functional chloroplasts and similar photosynthetic performance in both white areas and green areas of a variegated leaf. However, the detailed morphological differences between the variegated and green forms have not been examined previously. The aims of this work are to elucidate morphological differences between green (G) and variegated leaves (VW, white areas and VG, green areas) and reproductive differences between variegated (V) and green forms with a view to understanding fitness differences between the two forms.

Leaves, male flowers and fruits of *B. formosana* were collected at Wulai and the Yangmingshan National Park. The micromorphological traits of leaves, pollen and seeds were observed with a tabletop microscope. The results showed that the polygonal-shaped adaxial epidermal cells significantly vary in size (VG > G > VW). There is no size difference between guard cells of different leaf areas, but the VG area has the smallest subsidiary cells, and the VW area has the lowest stomatal density. The variegated form has significantly bigger pollen gains and significantly bigger seeds than the green form, but there is no difference in male flower size. These reproductive differences may reflect higher photosynthetic reserves of the variegated form, potentially due to lower herbivory on the variegated plant, allowing it to produce larger pollen grains and fruits.

KEYWORDS: adaxial epidermal cell, *Begonia formosana*, guard cell, male flower, pollen grain, seed, stomata, variegation

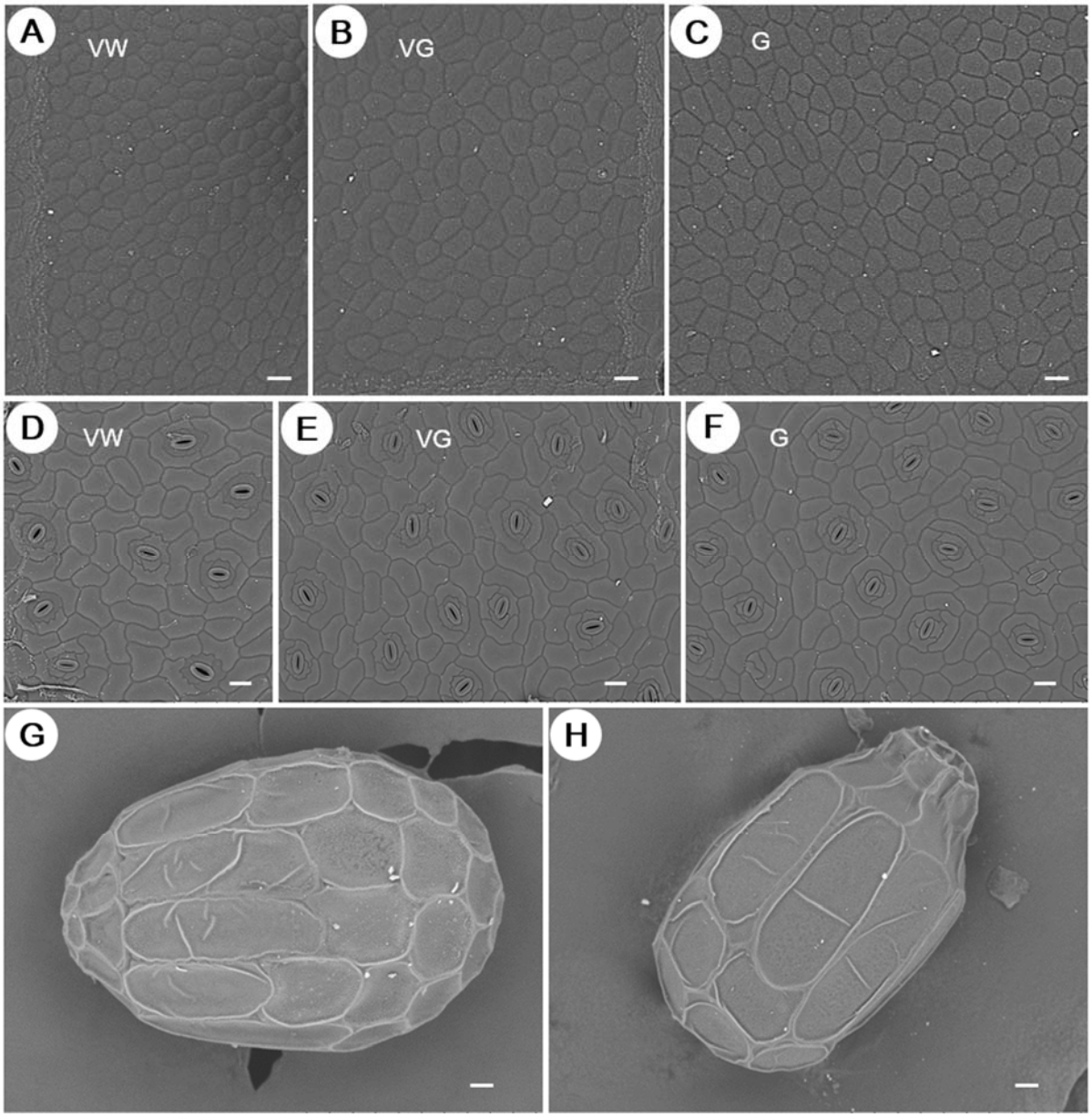

Figure 1. Leaf and reproductive characteristics in *Begonia formosana*. A-C: the adaxial epidermal cells in the three different areas of leaves. D-F: the stomata in the three different areas of the abaxial leaves. G: a seed of the variegated form. H: a seed of the non-variegated form. Abbreviations, VW: the white area of a variegated leaf; VG: the green area of a variegated leaf; G: a green leaf. Scale bars: A-F = 50 μm; G, H = 20 μm.

References

1. Hara, N. 1957. Study of the variegated leaves with special reference to those caused by air spaces. Japanese journal of Botany 16: 86-101.
2. Sheue, C. R., S. H. Pao, L. F. Chien, P. Chesson, and C. I Peng. 2012. Natural foliar variegation without costs? The case of *Begonia*. Annals of Botany 109: 1065-1074.

Abstract-B-02

Chloroplast diversity in the ancient genus *Selaginella*

Chiou-Rong Sheue (許秋容)[1], Peter Chesson[1, 2], Shau-Fu, Li (李紹輔)[1], Jian-Wei Liu (劉鑑緯)[1] and Chun-Lin Huang (黃俊霖)[3]

[1]Department of Life Sciences, National Chung Hsing University, Taiwan;
[2]University of Arizona, USA
[3]National Museum of Natural Science, Taiwan

In the dominant vascular plant clades, fully photosynthetic chloroplasts have highly conserved structure, severely limiting opportunities for comparative studies of chloroplast traits and their associated photosynthetic functioning. However, within the genus *Selaginella*, which originated in the Devonian in the most basal vascular plant division, Lycophyta, high chloroplast diversity is known, including major variations on chloroplast size and shape, ultrastructure, tissue location and number per cell. High diversity is also known from algae, and the diversity in *Selaginella* might be assumed to represent early diversification from an ancestral condition different from the typical vascular plant. This situation would limit their relevance to understanding potential adaptive constraints arising from in the dominant vascular plant clades. Here we show that the ancestral chloroplast condition in *Selaginella* is the typical condition for vascular plants, likely reflecting a common ancestor of all vascular plant chloroplasts. We provide evidence that major environmental changes over hundreds of millions of years have influenced *Selaginella* chloroplast diversification along different paths in different major regions of the Earth, with much present day chloroplast diversity arising relatively recently in the Cenozoic. This diversity includes monoplastidy, i.e. a single giant chloroplast per cell, which is strongly associated with deep shade habitats, and is further diversified with major variations on morphology and ultrastructure often found in different tissues of a leaf. This chloroplast diversity has the potential to provide major lessons on photosynthesis not available from typical model plant groups.

KEYWORDS: adaxial epidermal cell, bizonoplast, chloroplast, microphyll, monoplastid, Lycophyta, phylogeny

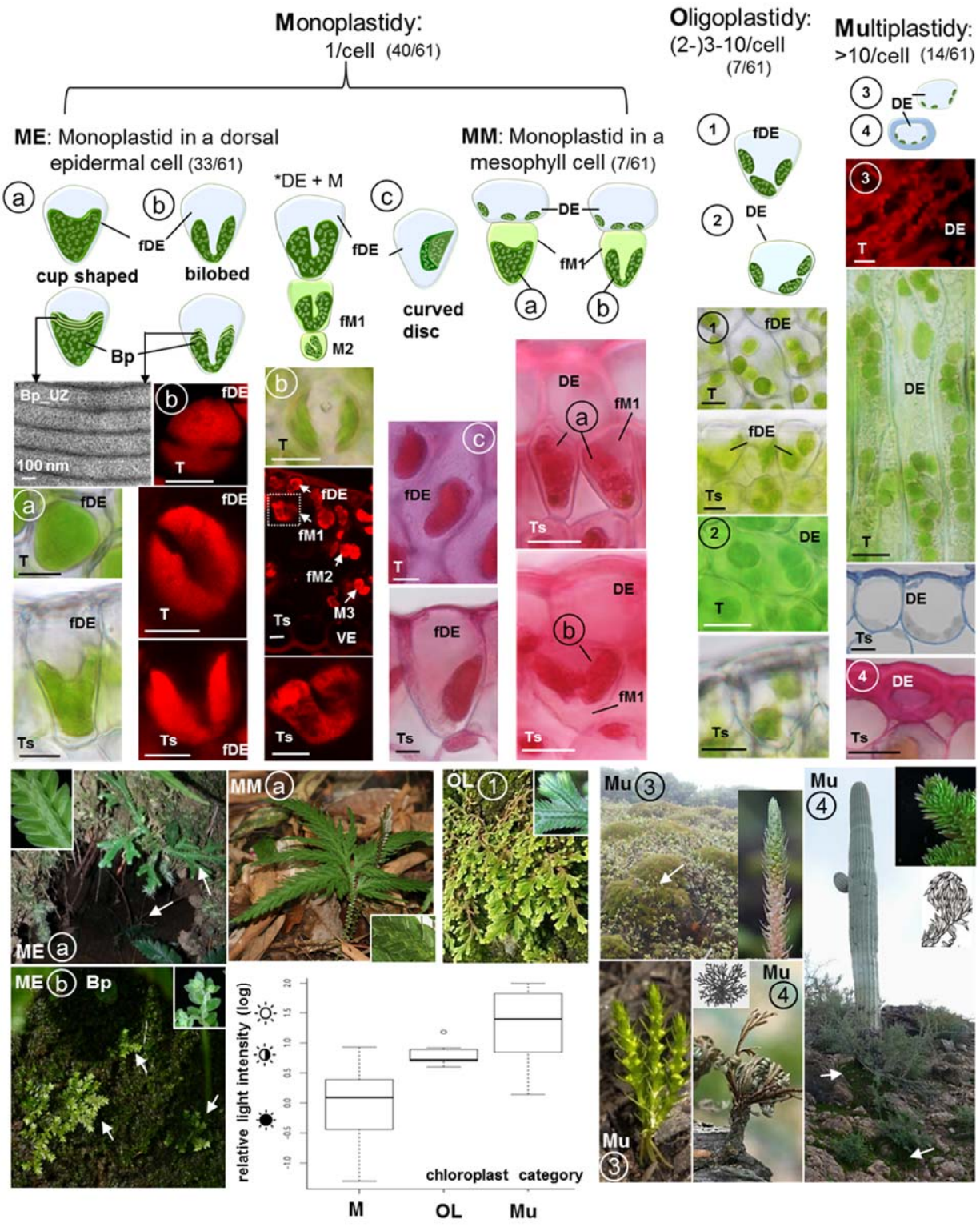

Figure 1. Chloroplast type, plant morphology and light environments. The graph of relative light intensity against chloroplast category shows that the species with monoplastidy (M) occur in deep shade environments in forests.

References

1. Sheue, C. R. et al. American Journal of Botany 94, 1922-1929 (2007).

Abstract-B-03

Micrographic Analysis of Sodium Chlorine-treated *Aedes aegypti* Eggs

Ling-Wei Weng (翁淩維) [1*], Hsiang-Ting Huang(黃祥庭)[1], Da-Syuan Yang(楊達璿)[1], Shiang-Jiuun Chen(陳香君)[2], Rong-Nan Huang(黃榮南)[1]

[1]Department of Entomology, National Taiwan University, Taipei, Taiwan

[2] Department of Life Science, College of Life Science, National Taiwan University, Taipei 10617, Taiwan

[*]r05632001@ntu.edu.tw

Mosquitoes are not only important vectors for many pathogens, their bites also cause allergic reactions in sensitive individuals. In addition to eliminate mosquito breeding sites (source reduction), synthetic insecticides are also periodically applied for vector control. However, it still cannot effectively suppress the outbreak of vector-brone diseases in Taiwan. It is therefore necessary to develop supplemental strategies for mosquito control. The eggs of mosquito does not receive much focus as the control target as that of larvae and adult stage. However, the egg shell could protect *Aedes* embryo from desiccation for 6 to 12 months (but not in *Culex* mosquito), and can hatch soon after rainfall, it should be the vulnerable stage suitable for mosquito control. Soon after oviposition, the chorion of mosquito egg becomes hardening and darkening, a melanization process that made the eggs highly resistant to desiccation. The current study showed that the hardening and darkening of *Ae. aegypti* egg were significantly inhibited by various salt ranging from 0.3M to 0.5M, which render the eggs futile. Micrographic analysis suggested that though the exochorionic network formed as usual, the morphology of NaCl-treated eggs were shrink and the number of peripheral tubercle were less than that of untreated eggs. Ultrastructural sections also showed that the exochorione layer did not firmly attach to endochorion in NaCl-treated eggs and their endochorion were thinner than that in control eggs. Whether the morphological distortion are responsible for the abnormal melanization and futile in the NaCl-treated eggs deserves further investigation.

References

1. Farnesi LC, Vargas HCM, Valle D, Rezende GL. 2017. Darker eggs resist more to desiccation: the case of melanin in *Aede*, *Anopheles* and *Culex* mosquito vectors. bioRxiv.
2. Li J. 1994. Egg chorion tanning in Aedes aegypti mosquito. Comparative biochemistry and physiology. Part A, Physiology 109:835-843.

INTEGRATED SERVICE TECHNOLOGY
宜特科技股份有限公司

TEM材料分析
技術能量達原子級之實驗室

先進製程檢測
最佳解決方案

應用領域:
IC產業、LED產業、面板產業、TFT-LCD產業、
太陽電池產業、奈米材料研究等。

宜特材料分析三大保證:

1. 已完成知名晶圓廠, LED磊晶廠和面板廠的分析試樣，獲得客戶肯定與高度評價。
2. TEM權威鮑忠興等多位博士專家，為您提供最頂尖的服務。
3. 全天候三班制24小時運作，全面縮短交期，產能大躍進。

Advanced Logic Device Analysis

High resolution TEM/EDS analysis on advanced MOS devices

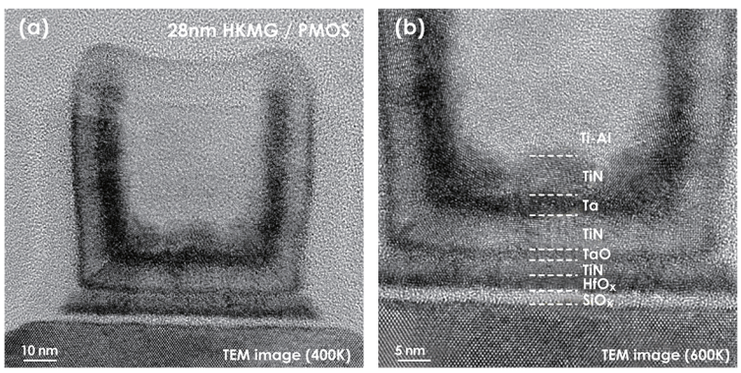

Figure (a) and (b): BF TEM image of a 28nm HKMG PMOS device.

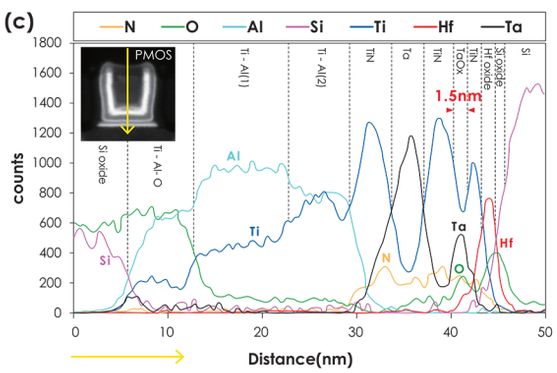

Figure (c): EDS lin-scan results of the gate stack. The 1.5nm-thick Ta layer can be well examined.

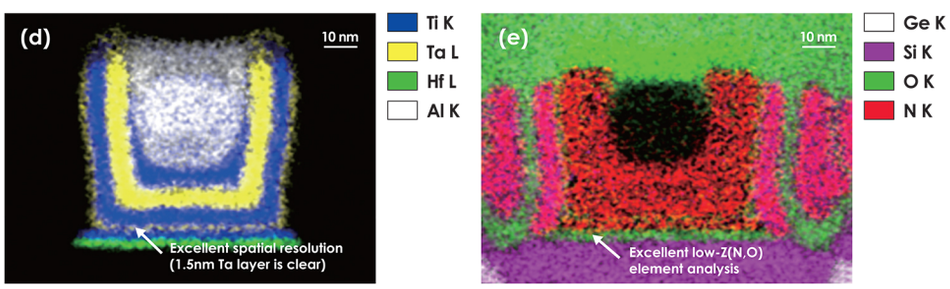

Figure (d) and (e) : EDS mapping results of the 28nm HKMG PMOS device. The 1.5nm-thick Ta layer and some O and N-contained layers can be well examined.

*以上影像皆由JEOL JEM-2800 場發射TEM機台取得。

洽詢專線 | iST 宜特科技 | Mr. Jeremy Chen | +886-3-579-9909 #8866 | Sales@istgroup.com

www.istgroup.com

Apreo
The most versatile high-performance FEG SEM

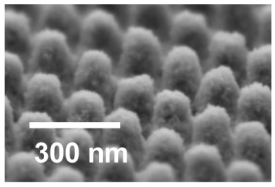

Best resolution on tilted or topographic samples

- Compound final lens
- 1.0 nm @ 1 kV (no BD required)

Best analytical performance

- Multiple EDS possible
- Coplanar EDS/EBSD
- 400 nA beam current
- LoVac compatible

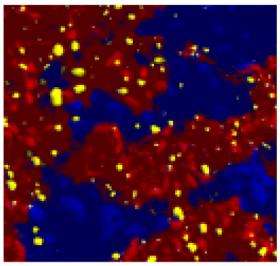

The best contrast under practical conditions

- T1: in-column, high signal

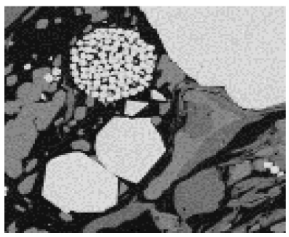

The New S/TEM Talos™ F200X

Highest resolution and throughput in STEM imaging
Fastest and precise EDS analysis in all dimensions (1D-4D)

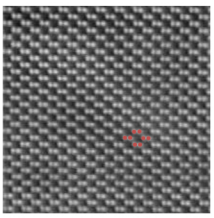

EDS 3D of light elements:
Elemental distribution within the acidocalcisome matrix
P **Ca** **Mg**

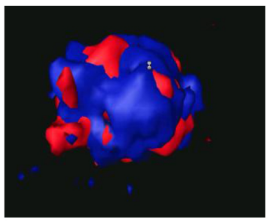

ThermoFisher SCIENTIFIC
FEI™

超泰科技有限公司
E. B. TECH CO., LTD

台北市光復南路495號7樓之5
Tel: (02) 2729-5268
Mail:Tracy_Hsieh@ebtech.com.tw

第三十七屆臺灣顯微鏡學會年會攝影比賽影像集

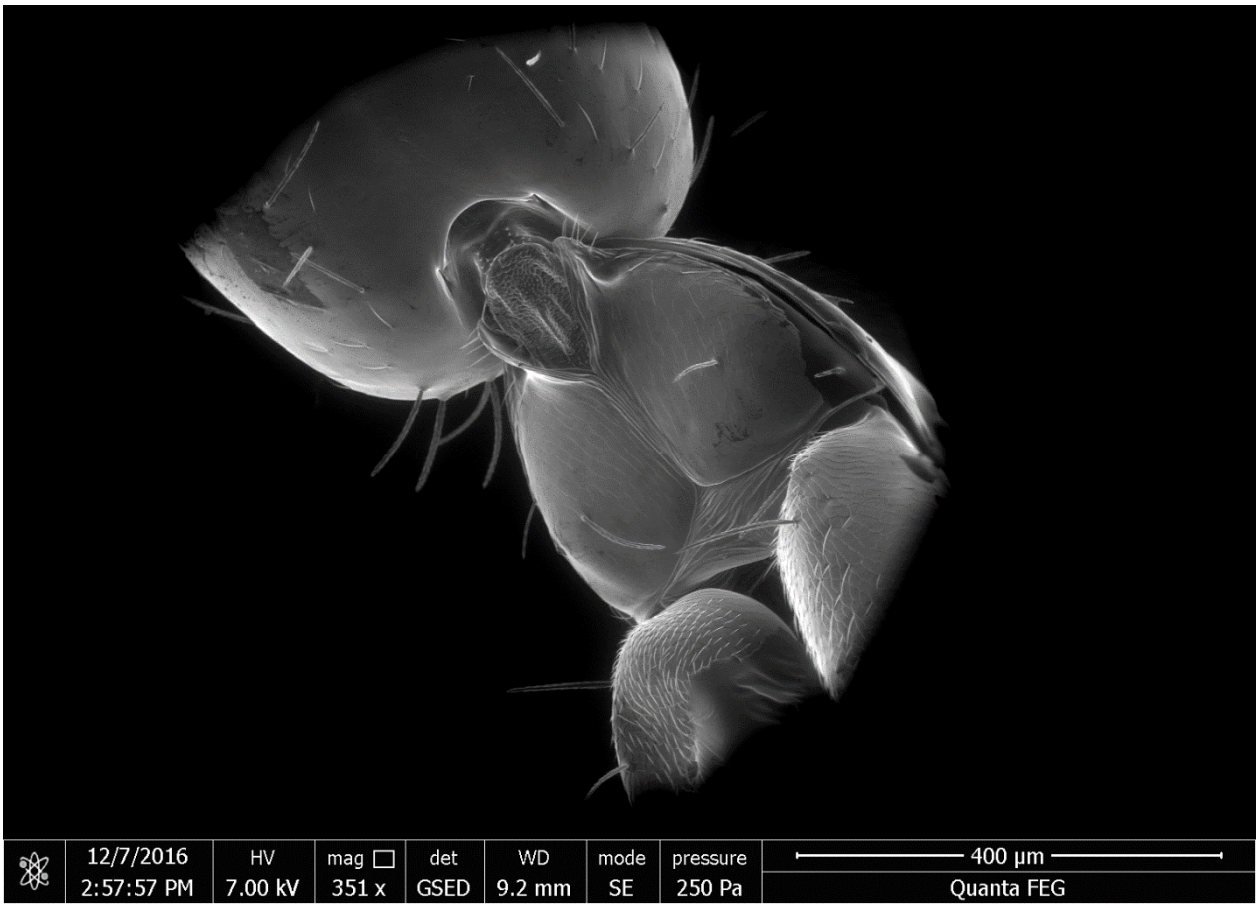

作品名稱：以管窺蟻

作品內容

透過電子顯微鏡觀察螞蟻形貌

作者姓名：高全盛、吳帝瑩

學校單位：台大材料所、台電樹林綜合研究所

E-Mail：D03527005@ntu.edu.tw

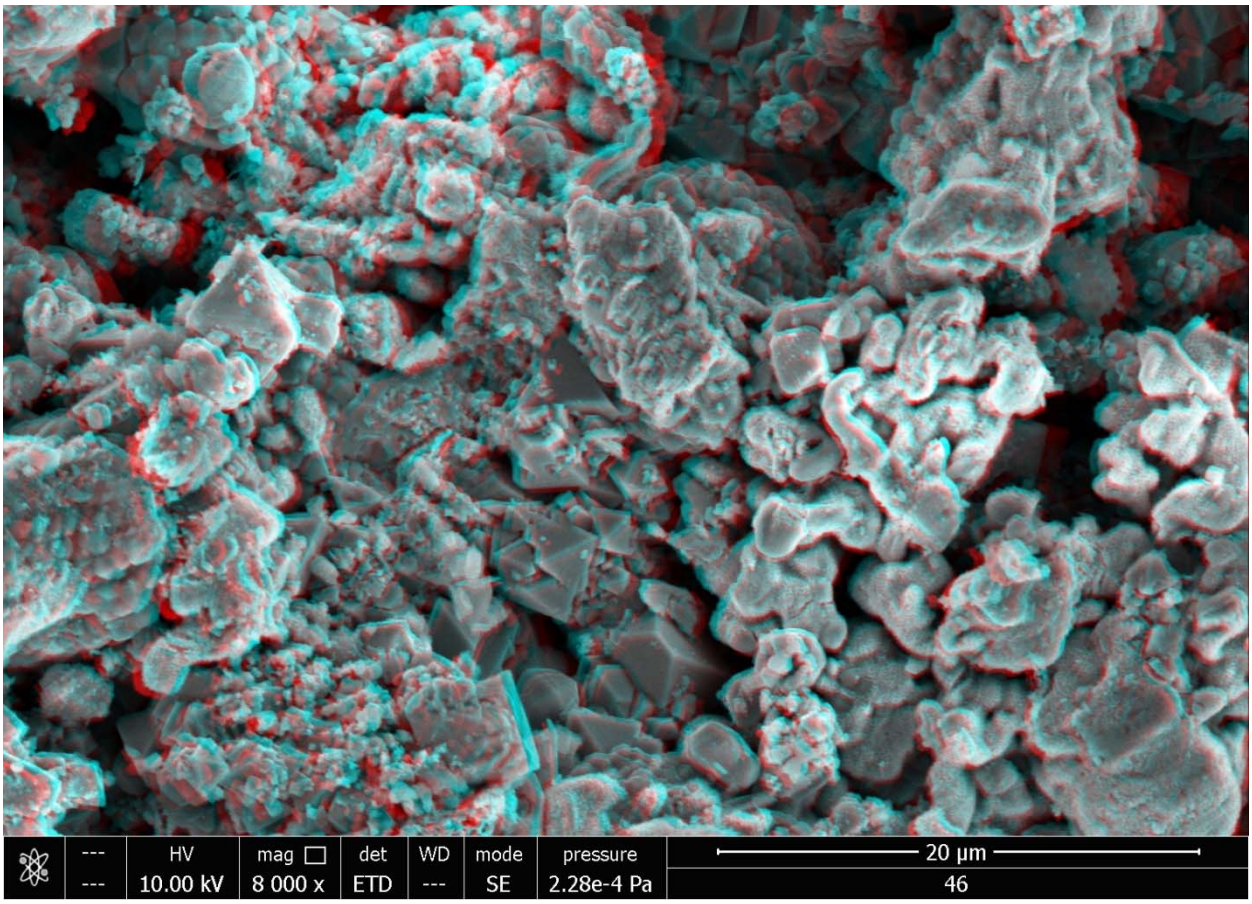

作品名稱：無底深淵

作品內容

透過電顯技術，以 3D 影像表達腐蝕孔洞。

作者姓名：高全盛、吳帝瑩

學校單位：台大材料所、台電樹林綜合研究所

E-Mail：D03527005@ntu.edu.tw

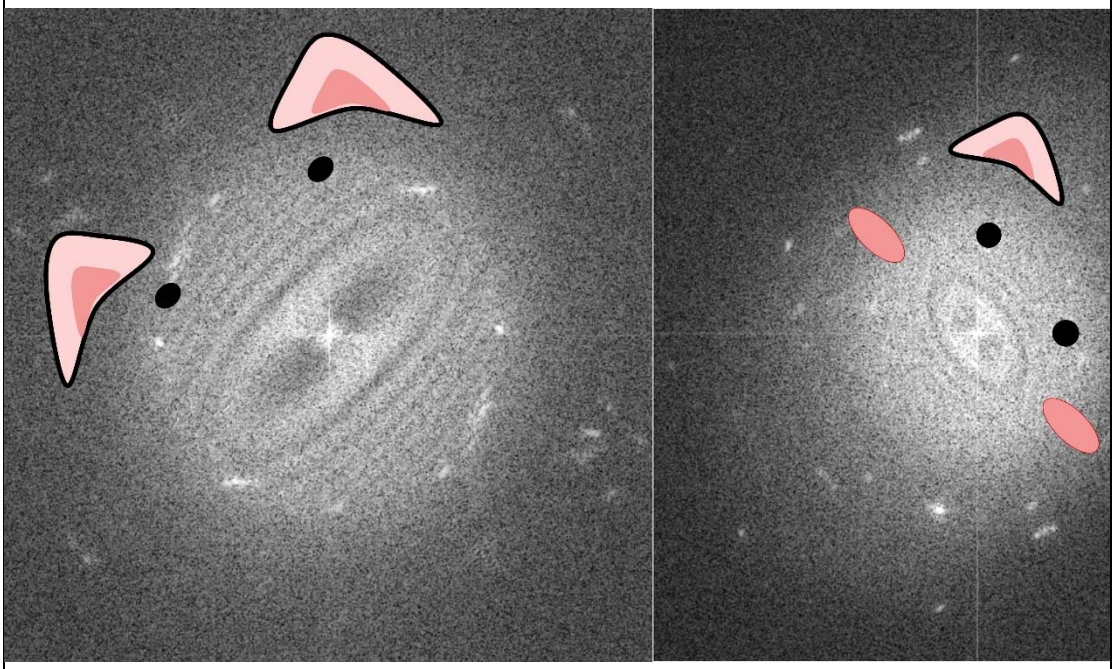

作品名稱　豬老爸與豬小弟

作品內容

Si 奈米顆粒具有非晶及部分結晶區域，將它的 HRTEM 影像經傅立葉轉換，得到豬鼻子影像。

作者姓名：蔡季霖	**學校單位：成功大學材料系**
E-Mail：haheart10@gmail.com	

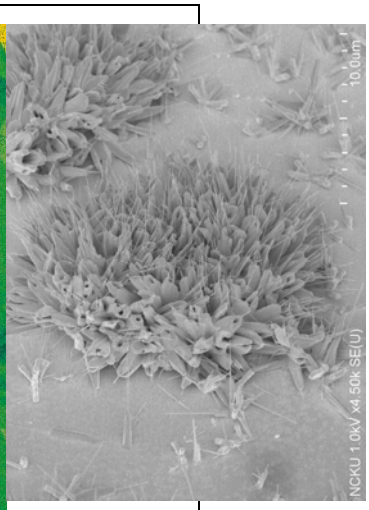

作品名稱　陶菊
作品內容 以氣相沉積法形成的 ZnO 奈米柱，堆積如秋菊般之清雅高潔，不禁讓人想到陶淵明「採菊東籬下」之景。

作者姓名 張乃云	**學校單位** **國立成功大學材料科學及工程學研究所**
E-Mail　wasvance@gmail.com	

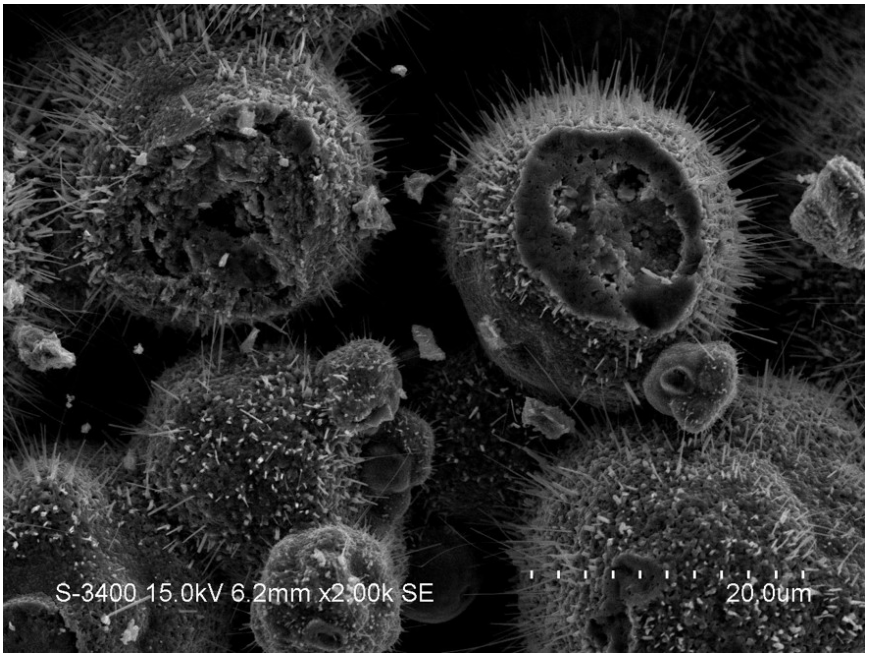

作品名稱: 勒索病毒-錢拿來

作品內容:
利用銅粉放入陶瓷舟，使用加熱板進行退火 12hr 550℃。(下方為 SEM 原圖)。

作者姓名: 林佳慶 邸心緯 張育誠

學校單位: 逢甲大學材料科學與工程學系

E-Mail: yvette831210@gmail.com

作品名稱　六芒星的詛咒

作品內容

鋼鐵中沃斯田鐵相在<3 5 6>正晶帶軸之 TEM 聚束電子繞射(convergent beam electron diffraction, CBED)圖樣，如同六芒星一般。

作者姓名 蔡世寧	**學校單位** 台大材料所

E-Mail r04527011@ntu.edu.tw

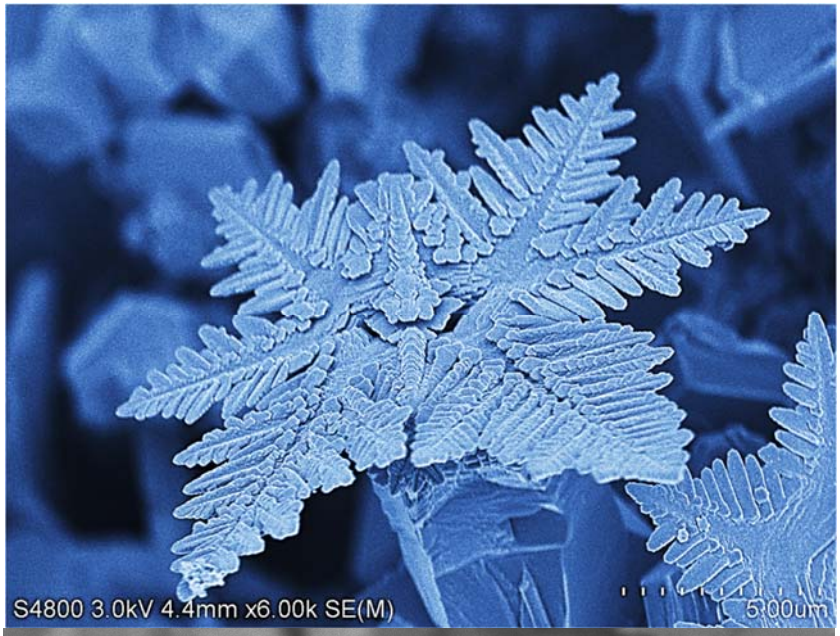

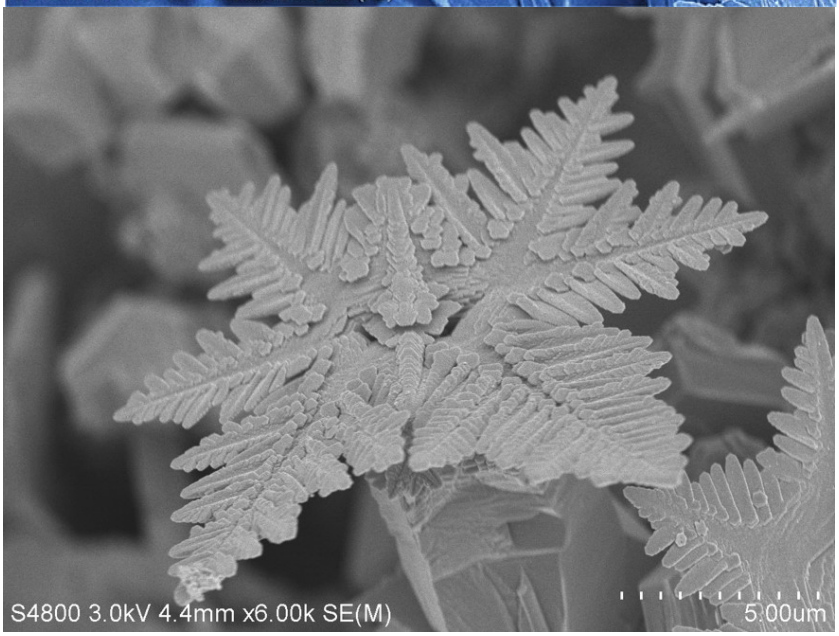

作品名稱 ： 楓霜冰晶	
作品內容 ： **紅銅片在加熱板上退火 6hr 550℃，之後透過水熱法生長 MoS_2。(下方為 SEM 原圖)。**	
作者姓名 ： 莊凱崴 邸心緯 張育誠	**學校單位 ： 逢甲大學材料科學與工程學系**
E-Mail : reation1506@gmail.com	

作品名稱　山中迷濛步道

作品內容

一個沃斯田鐵的雙晶，儼然就像是山中迷濛細雨的階梯步道，圖下端的黑影就像是一個句阿的腳印。

作者姓名 童博彥	**學校單位 台大材料系**
E-Mail r02527051@ntu.edu.tw	

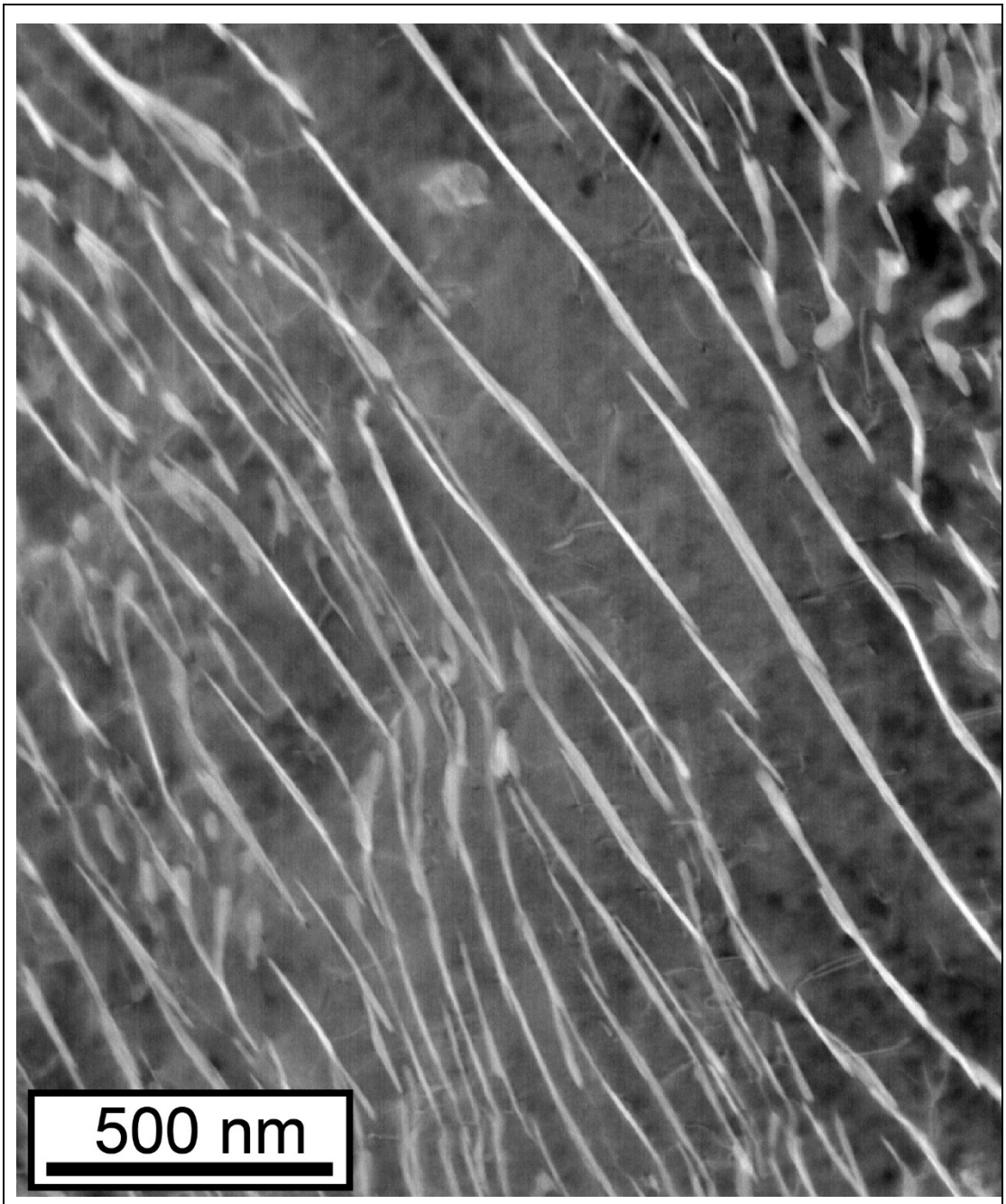

韌作品名稱　川流不息
作品內容：利用 STEM ADF 技術，拍攝波來鐵。波來鐵在肥粒鐵基地中，像湍急的水流與河岸邊的石頭撞擊，激起了美麗的渦流與水花。

作者姓名：陳昱文	學校單位：台大材料所
E-Mail：f01527051@ntu.edu.tw	

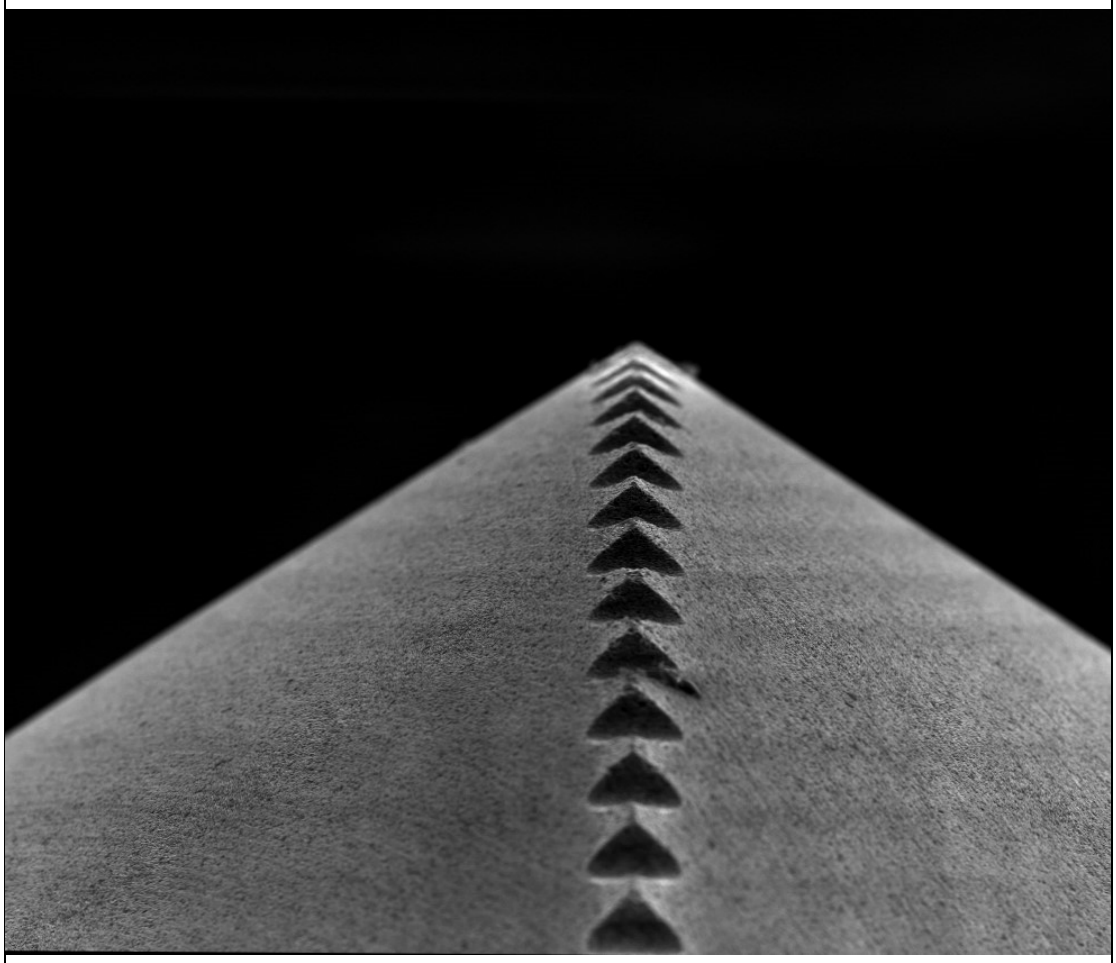

作品名稱 一條通往頂尖的路

作品內容 看似風光的頂端，都是一步一腳印，跨越重重關卡才能抵達的。
此為小型刀具的尖端。

作者姓名 賴世雯	**學校單位 台大材料所**

E-Mail:r04527006@ntu.edu.tw

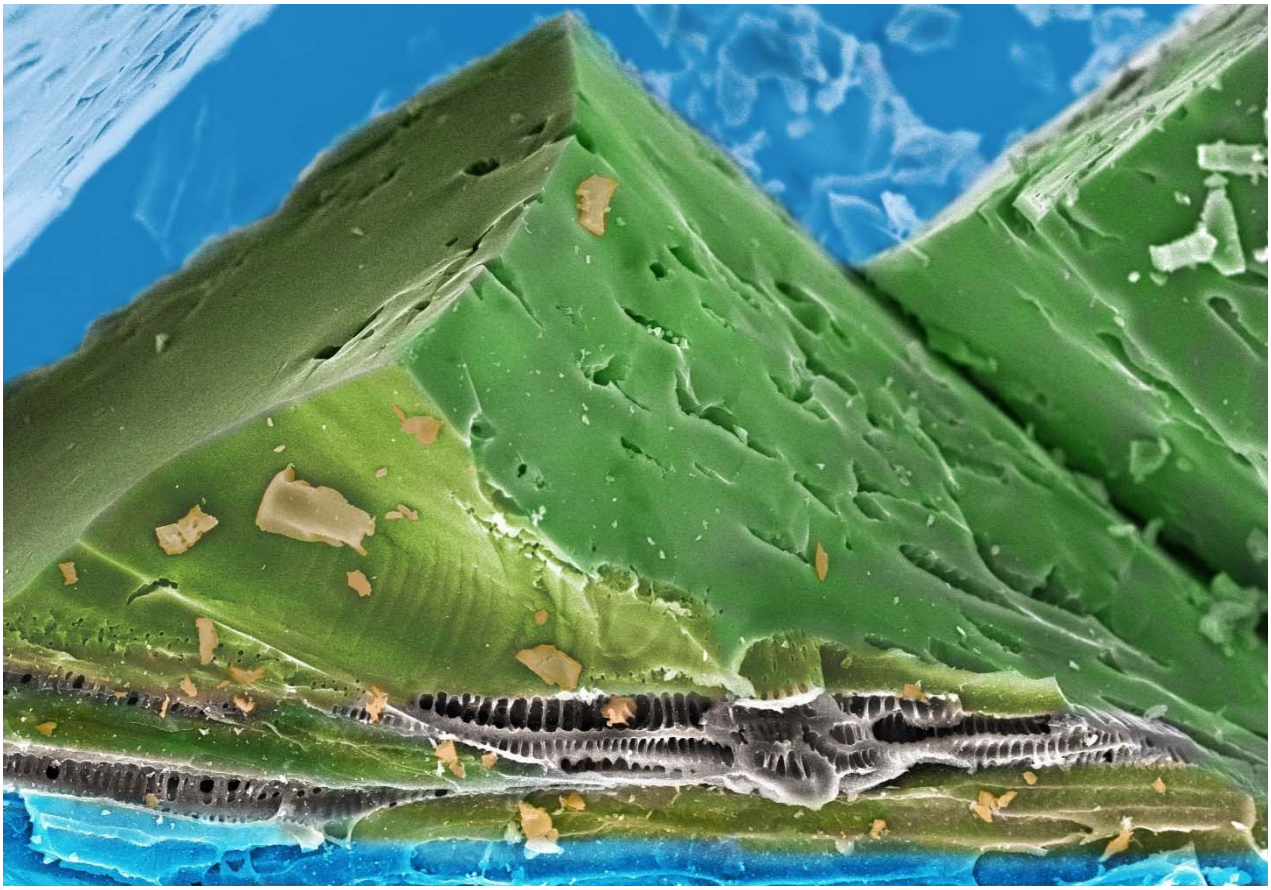

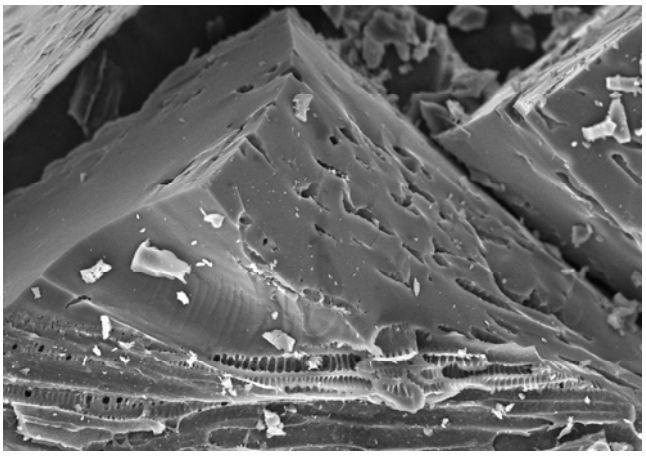

作品名稱: 看見臺灣

作品內容

多孔洞活性碳材在掃描式電子顯微鏡下觀察，如同蘇花公路間的明隧道，穿越沿海陡峭的山巒之間。

作者姓名: 黃冠銘、王惇平、廖英志	**學校單位: 國立臺灣大學化學工程學系**

E-Mail: r04524058@ntu.edu.tw

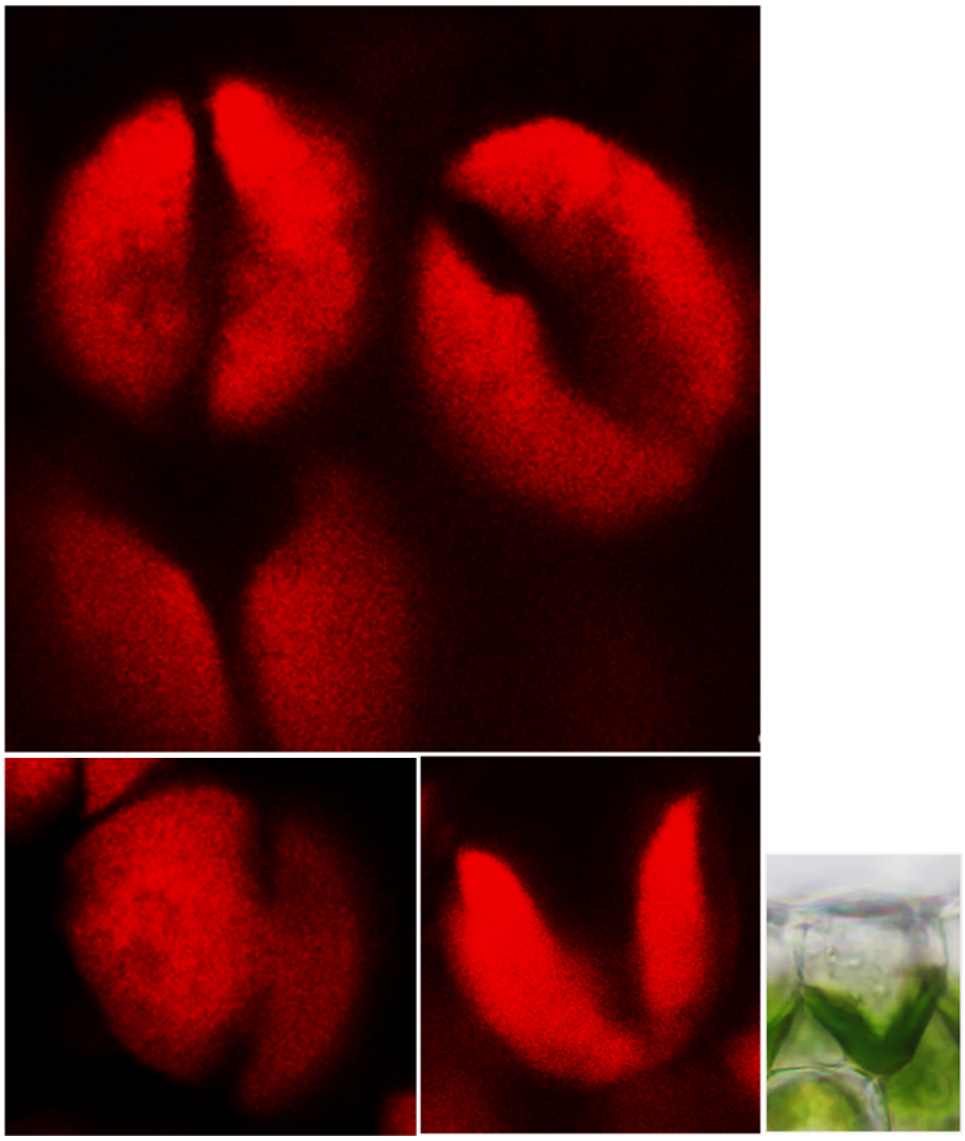

作品名稱　葉綠體之吻	
作品內容 **這是一種卷柏植物葉內所發現的巨大葉綠體，呈二深裂狀。在以共軛焦顯微鏡由上方看似一紅唇或鈕鈴形，側面則有如一鬱金香。**	
作者姓名　許秋容、李紹輔、劉鑑緯	**學校單位　中興大學生命科學系**
E-Mail　crsheue@gmail.com	

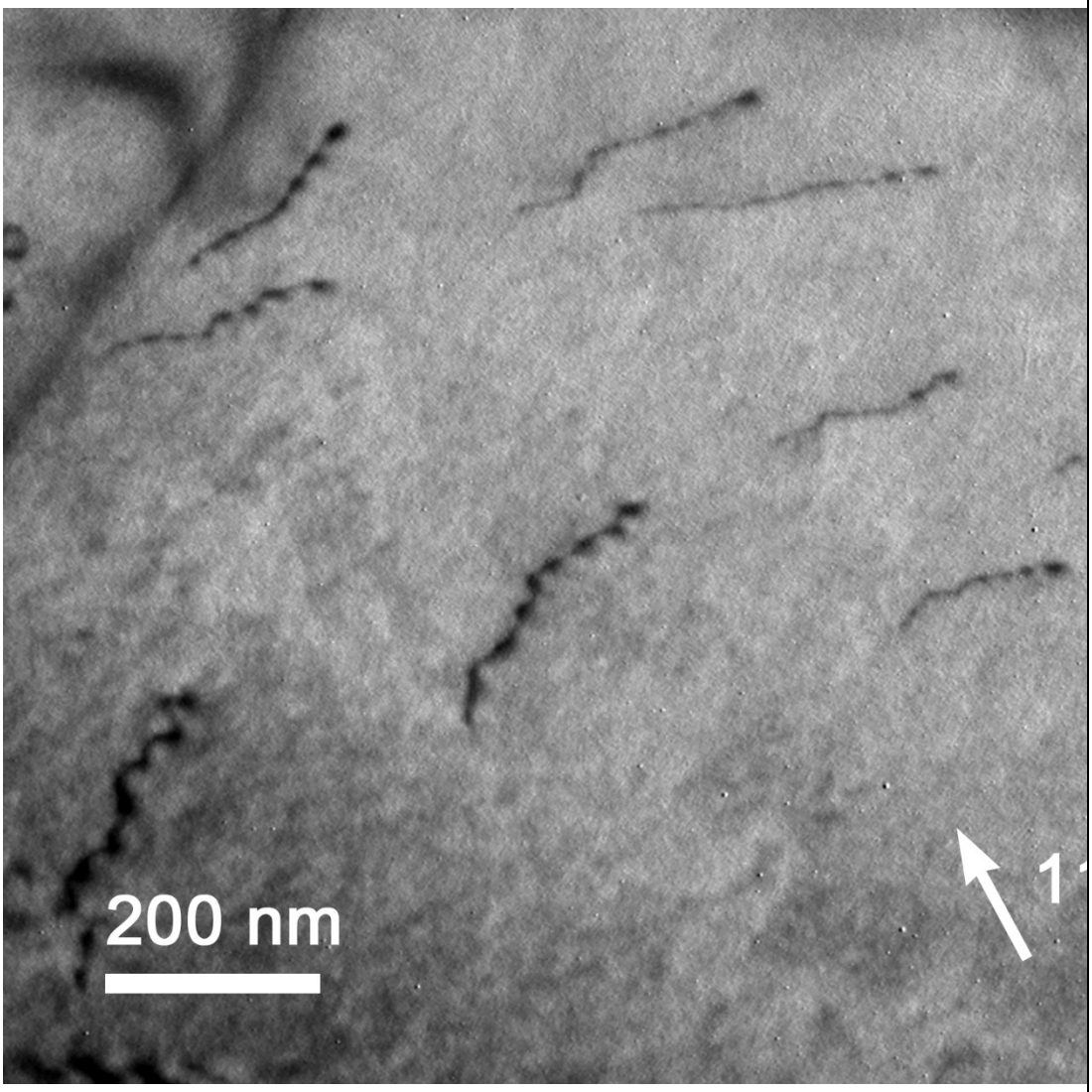

作品名稱:　生命之初

作品內容:

此為雙相鋼中肥粒鐵內部利用 TEM 明場雙束條件<110>拍攝出的 dislocation 樣貌。與生命之誕生有著不可分割的無限聯想。

作者姓名: 蔡劭璞　　**學校單位: 台灣大學材料所**

E-Mail: f01527016@ntu.edu.tw

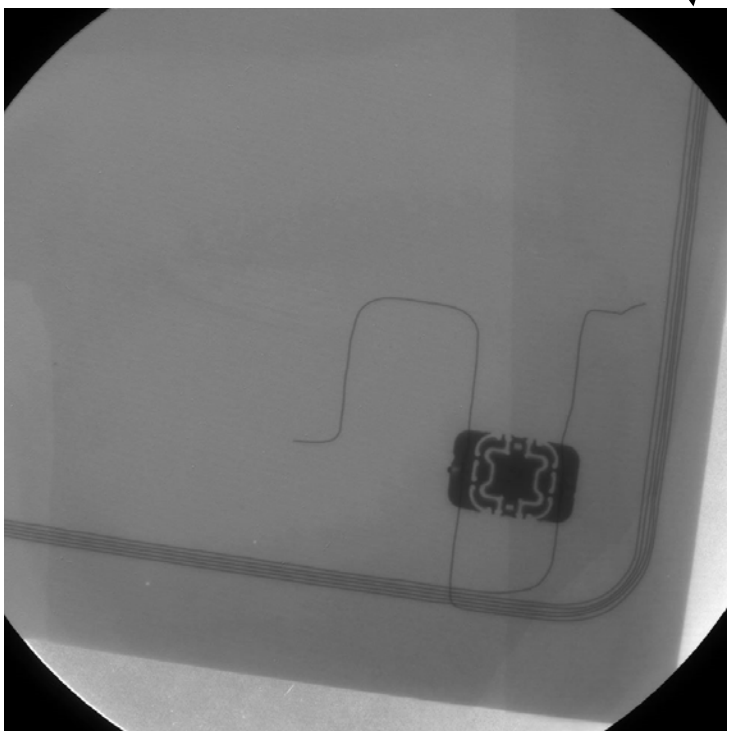

作品名稱:　我的 RFID

作品內容:

我的服務證以微聚焦 X 光機與 X 光 CCD 成像, 倍數 x10。RFID 還有天線，XRF 證實為銅線。

作者姓名: 李志浩

學校單位: 清華大學工程與系統科學系

E-Mail: chlee@mx.nthu.edu.tw

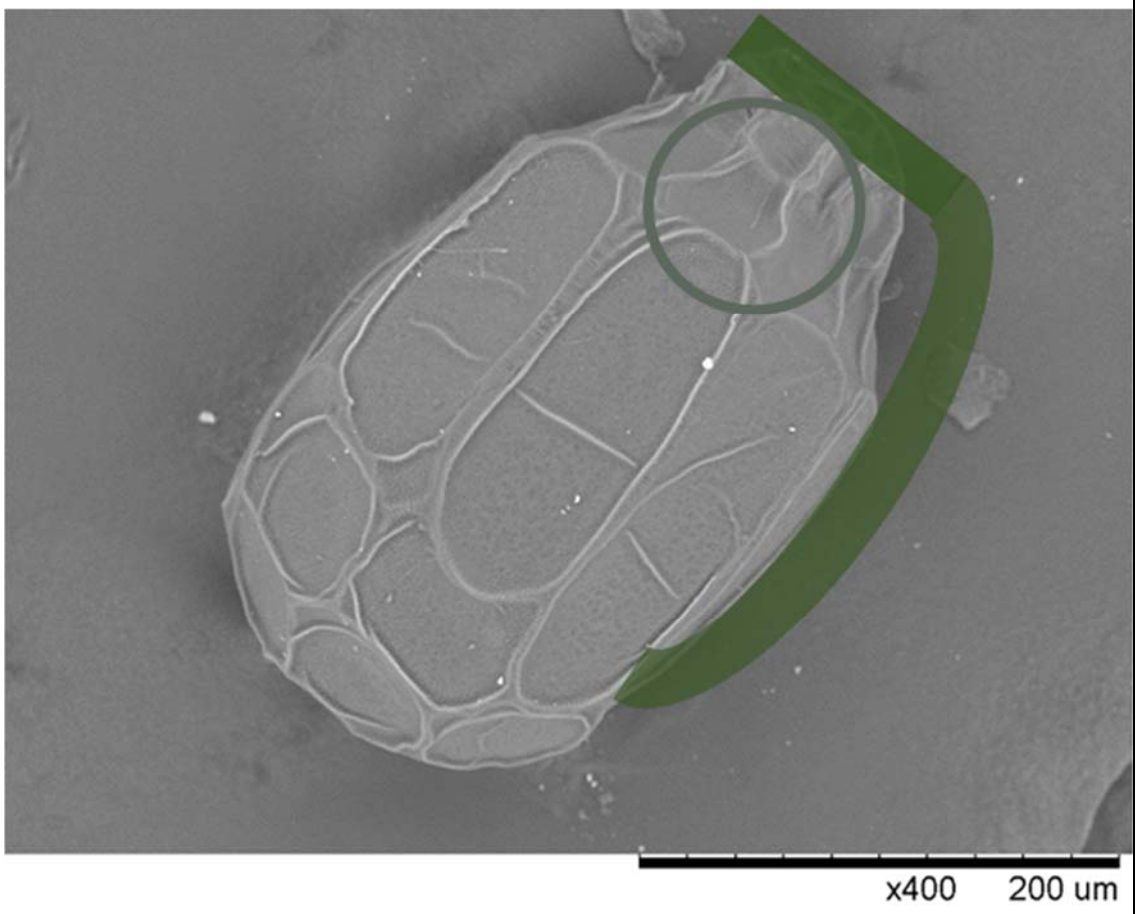

作品名稱 手榴彈爆炸

作品內容

插銷尚未拔出的手榴彈！趕快避難，小心別被水鴨腳秋海棠種子炸到啦！

作者姓名 林宜憲 | **學校單位** 中興大學 生命科學系碩士班

E-Mail: yamie801007@gmail.com

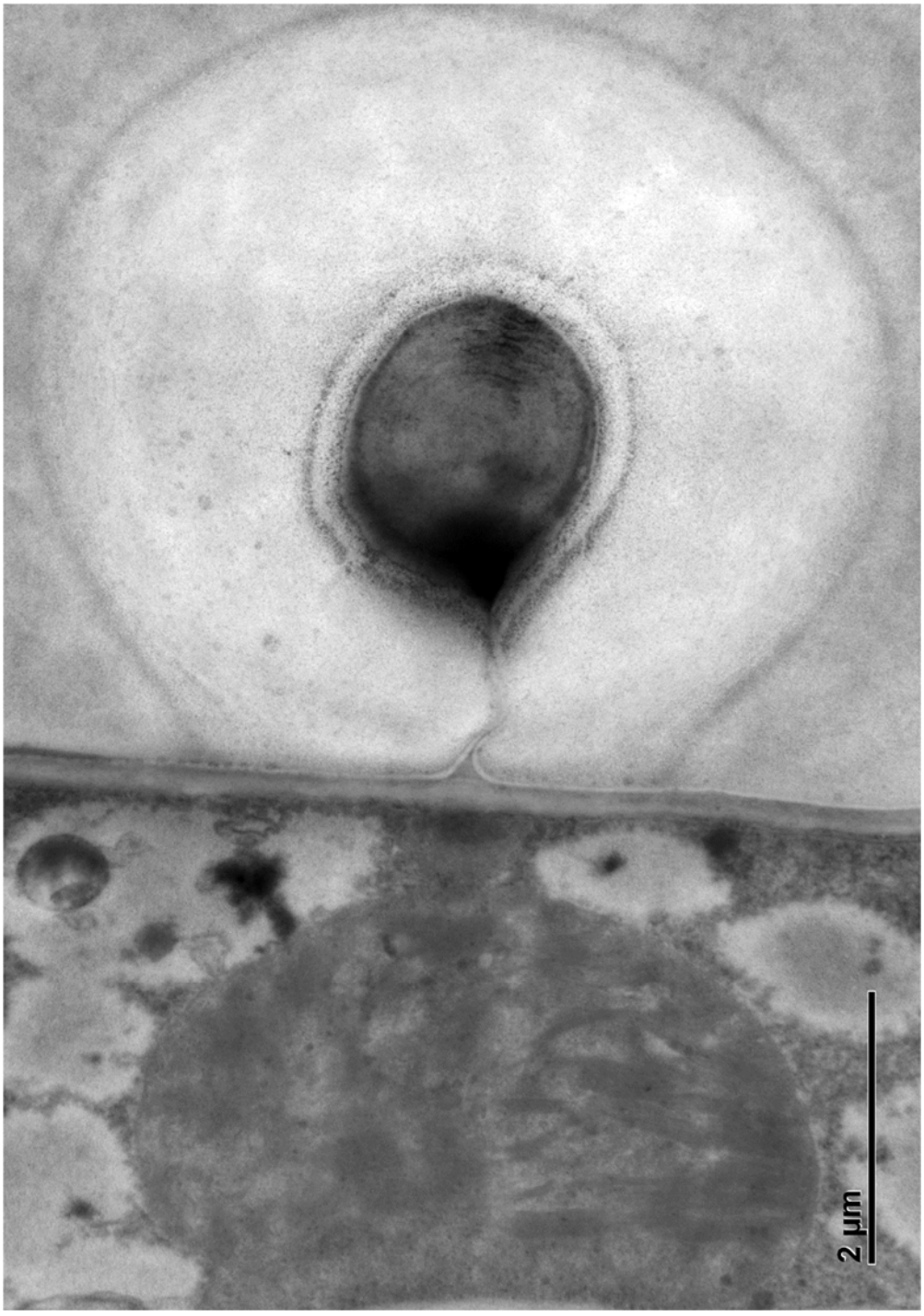

作品名稱　　平潭映月	
作品內容 此為植物葉片的切片結構，下半部為葉肉細胞與內含之葉綠體。	
作者姓名　劉鑑緯、許秋容	學校單位 國立中興大學生命科學系
E-Mail crsheue@gmail.com	

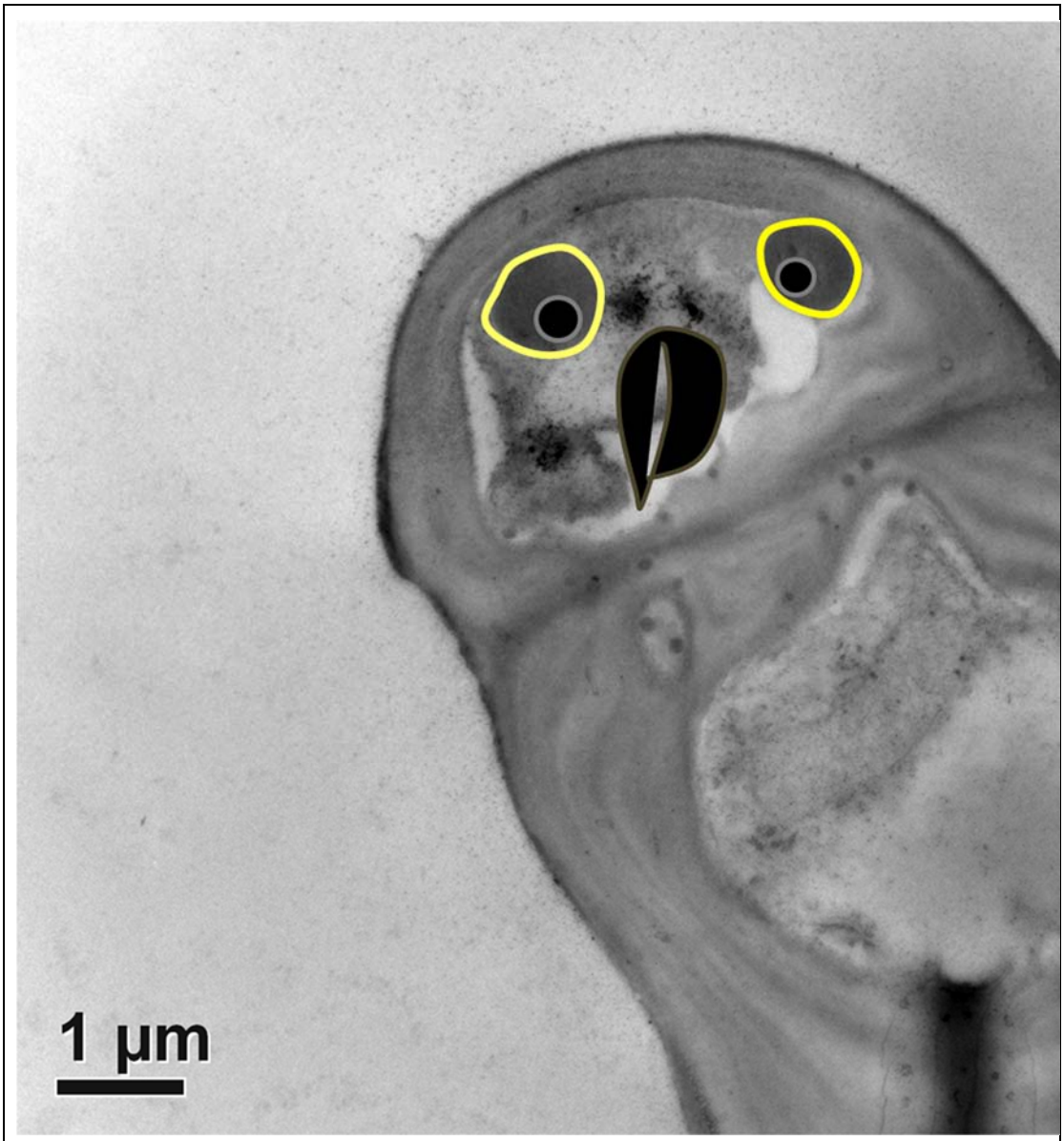

作品名稱　「嘿美 」	
作品內容 嘿美為哈利波特中-哈利的寵物白色貓頭鷹。此為卷柏葉片葉緣的橫切。	
作者姓名　劉鑑緯、許秋容	學校單位 國立中興大學生命科學系
E-Mail crsheue@gmail.com	

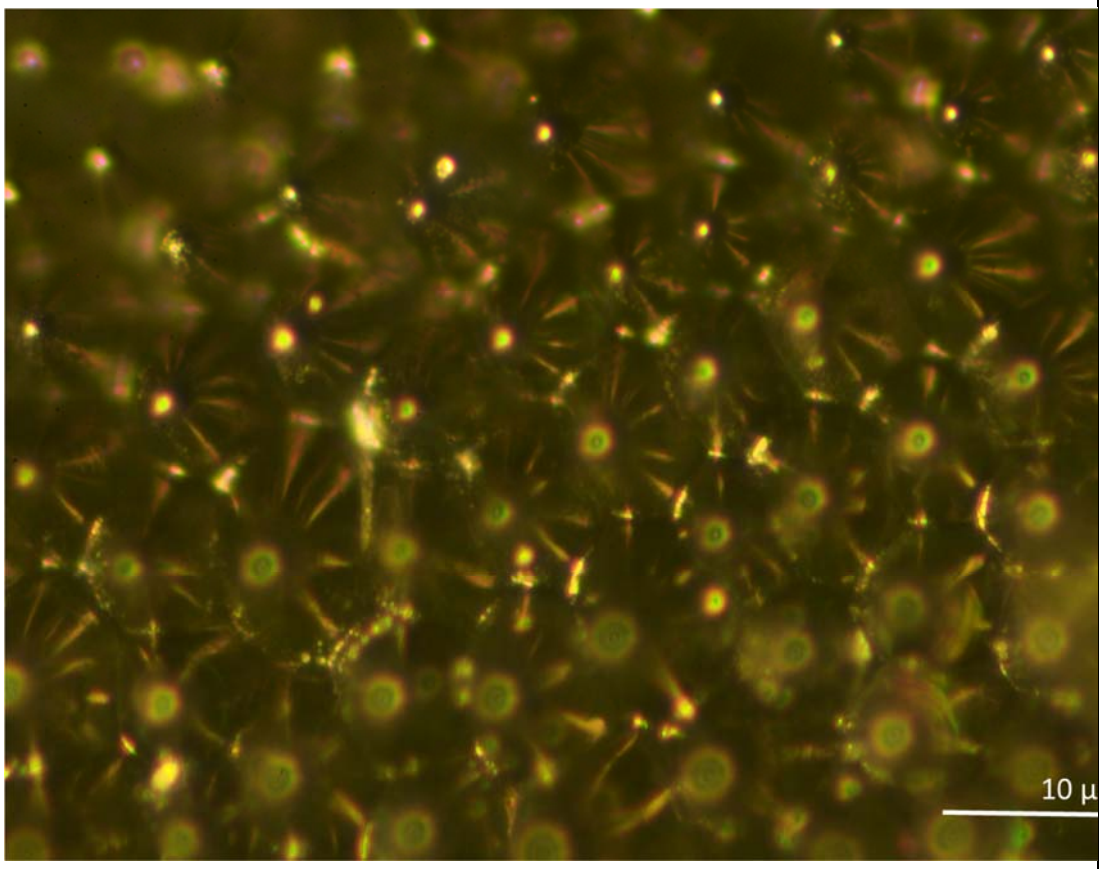

作品名稱　星空

作品內容

此為彩葉孔雀薑 (*Kaempferia pulchra*) 葉片近軸面墨綠色區域，以光學顯微鏡搭配反射光源觀察近軸面表皮細胞。

作者姓名　蔡秉芸、許秋容

學校單位　國立中興大學生命科學系

E-Mail　crsheue@gmail.com

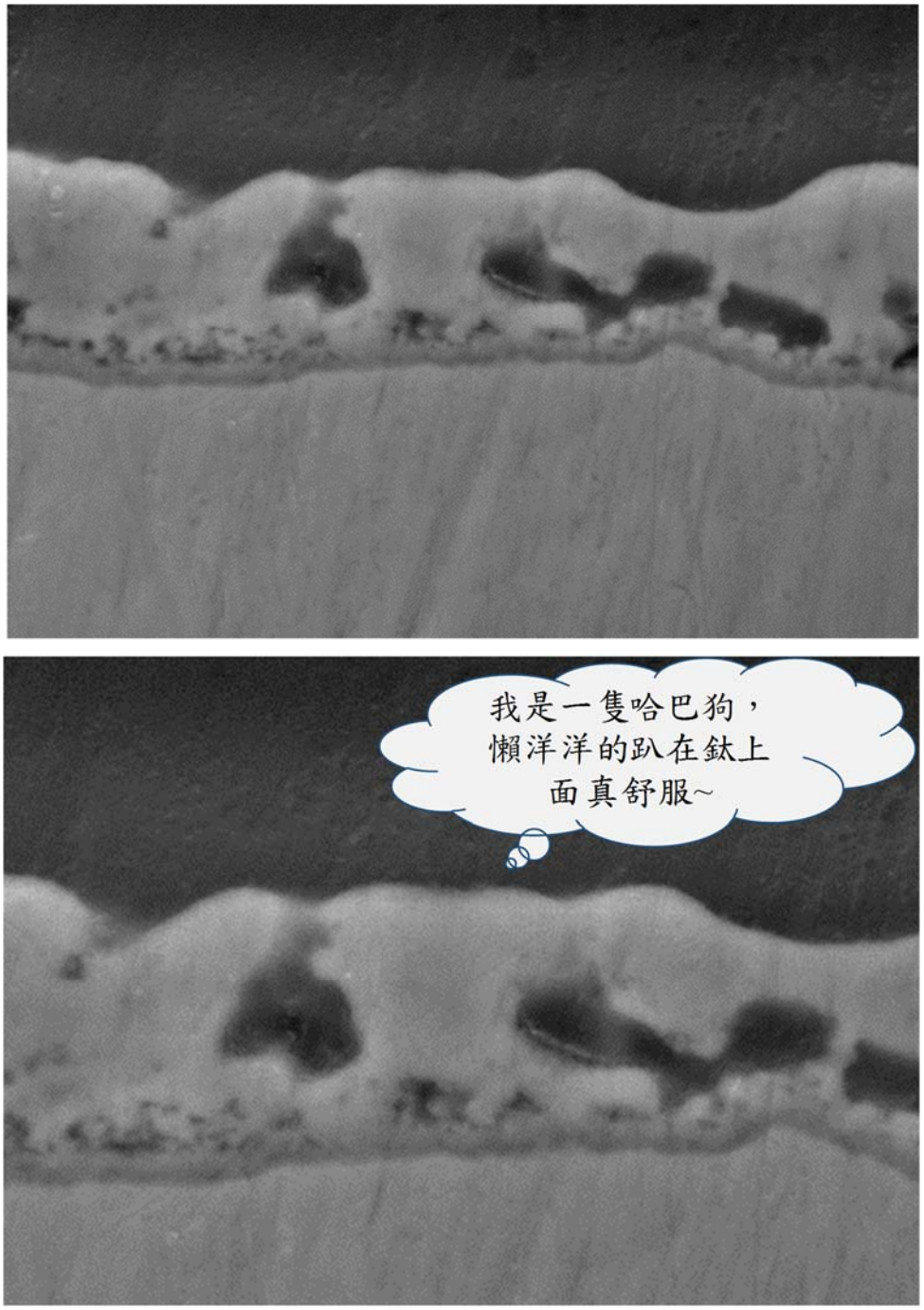

作品名稱： 鈦上哈巴狗

作品內容：

利用電漿電解氧化技術於純鈦基板上製備二氧化鈦薄膜，截面 SEM 影像貌似一隻哈巴狗懶洋洋地趴在鈦上面。

作者姓名: 鄭凱文、黃彥凱、曾傳銘 | **學校單位: 明志科技大學材料工程系**

E-Mail: m05188010@mail2.mcut.edu.tw

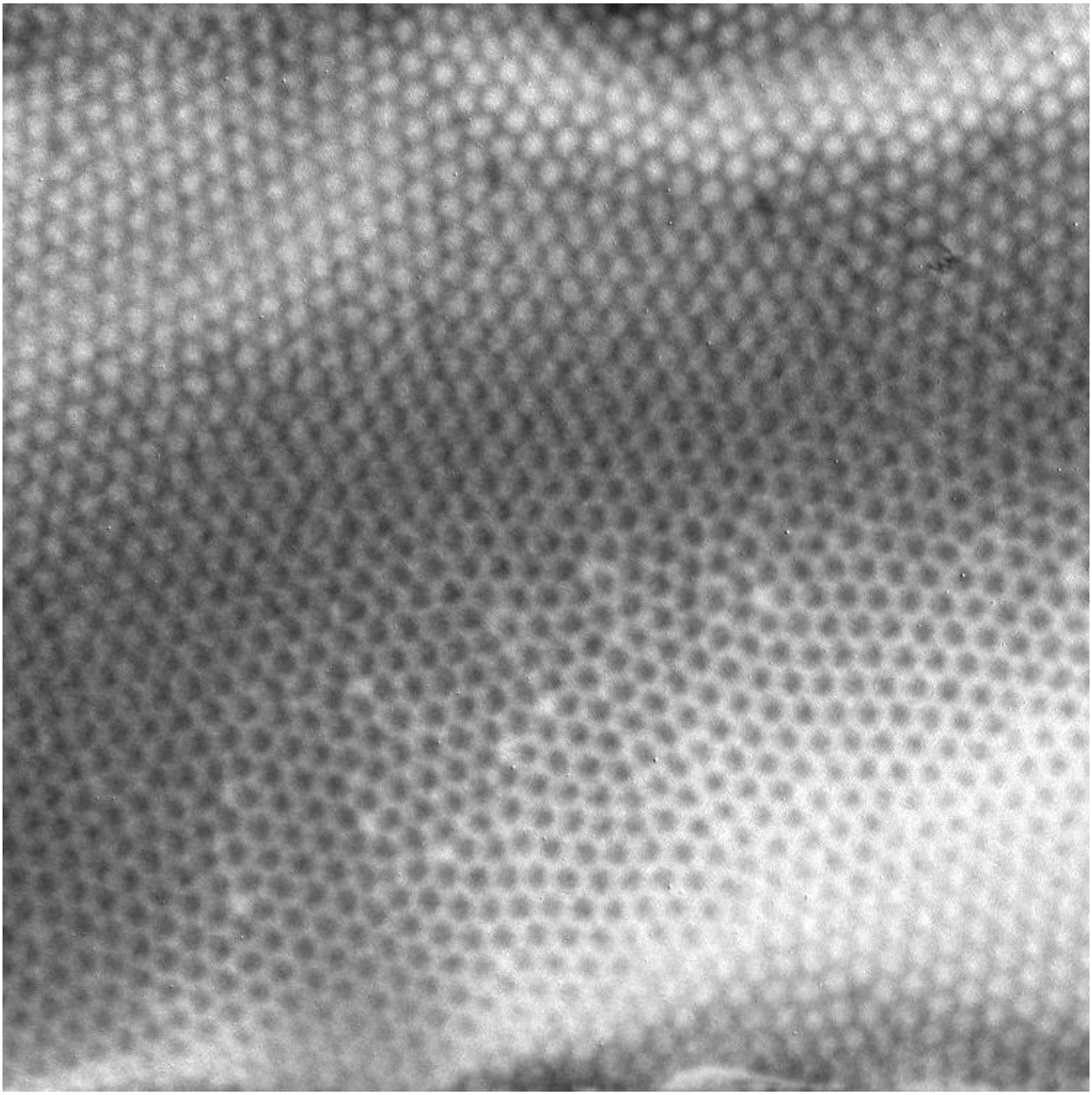

作品名稱　籃球紋
作品內容 **2205 雙相不鏽鋼在作電解拋光時，偶爾會出現的規綠條紋。**

作者姓名 蔡宇庭	學校單位 台大材料所
E-Mail: f99527004@ntu.edu.tw	

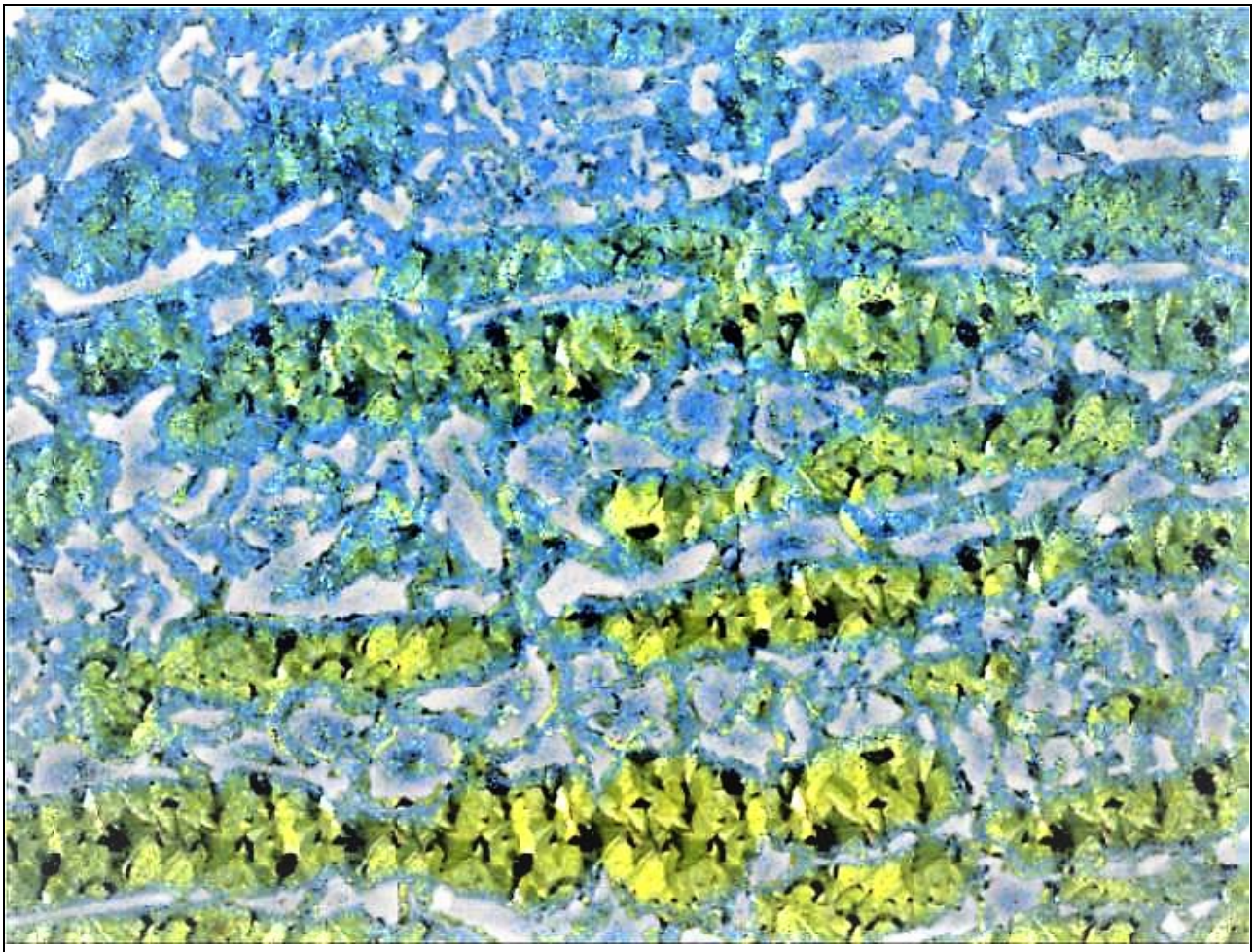

作品名稱　層巒聳翠間之冰河鳥瞰

作品內容

雙相不鏽鋼經熱循環處理後，δ-ferrite 相產生共析反應，為 3 種相 γ＋γ'＋σ 之組成。
猶如：層巒聳翠間之冰河鳥瞰。

作者姓名：　李建欣	**學校單位　：** **國立台灣海洋大學機械與機電所**

E-Mail 10272044@ntou.edu.tw

The new standard for FIB-prepared specimen preparation

United States Patent No. 7,132,673 No. 7,504,623

Model 1040 NanoMill®

- Ultra-low energy ion source
- Concentrated ion beam
- Removes amorphous and implanted layers
- Post-FIB processing and enhancement conventionally prepared specimens

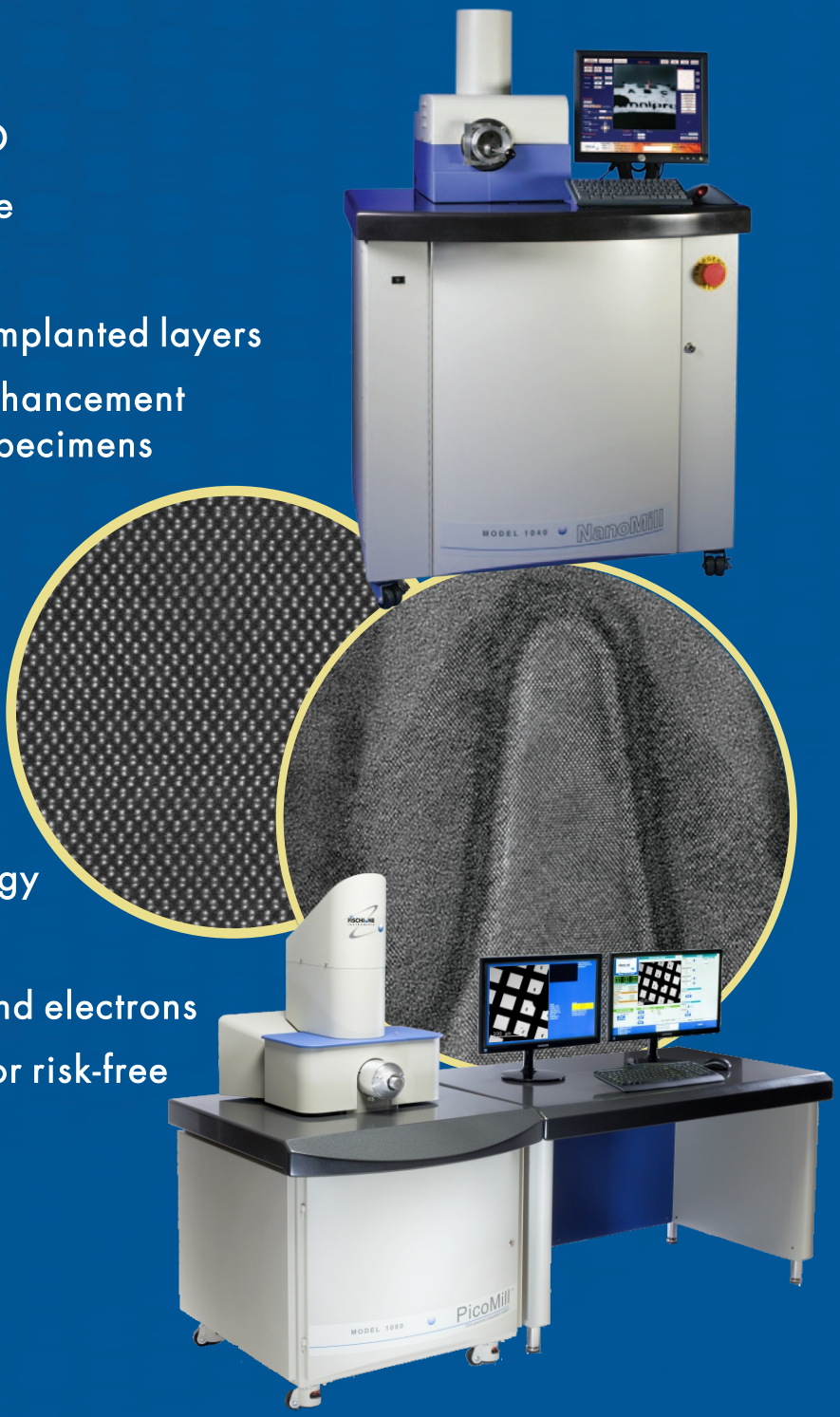

Model 1080 PicoMill®

- Concentrated ion beam
- Complements FIB technology
- Precise endpoint detection
- In situ imaging with ions and electrons
- Microscope connectivity for risk-free specimen handling

FISCHIONE INSTRUMENTS

SANPANY www.sanpany.com.tw
三朋儀器股份有限公司
台北市忠孝東路一段112號6樓 6F
TEL: (02)2392-3433

M1040 M1080

INNOVATION

Pioneering Nanoanalysis Solutions

Advanced solutions for the SEM, TEM and FIB

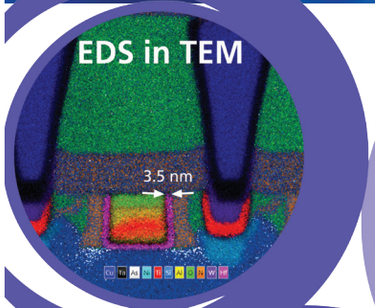

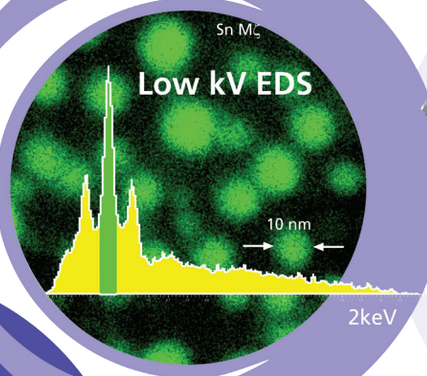

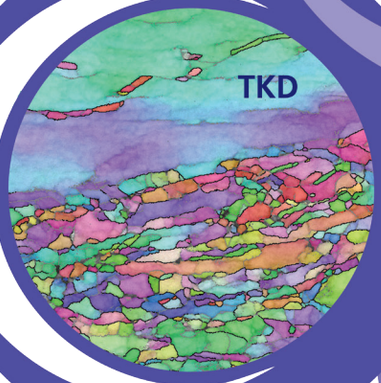

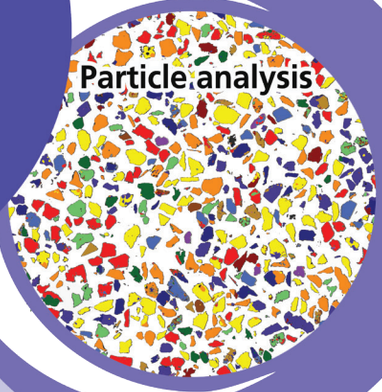

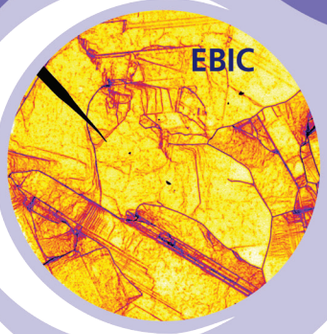

We provide leading-edge tools for advanced elemental, phase, microstructure and electrical nanoanalysis

- EDS from large area mapping to atomic column analysis
- Low kV and light element analysis
- Grain analysis at the micro- and nanoscale using EBSD & TKD
- Automated particle analysis and gunshot residue analysis
- Lamella preparation
- EBIC and EBAC studies

www.oxford-instruments.com/nanoanalysis

OXFORD INSTRUMENTS

The Business of Science®

FEI
part of Thermo Fisher Scientific

Helios PFIB

A revolution in sample prep & analysis: millimeters to nanometers

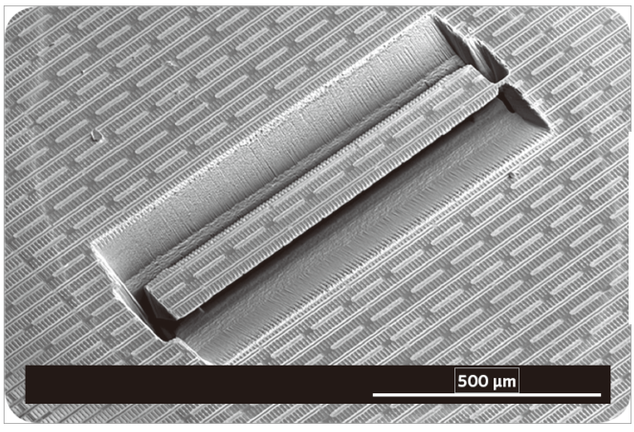

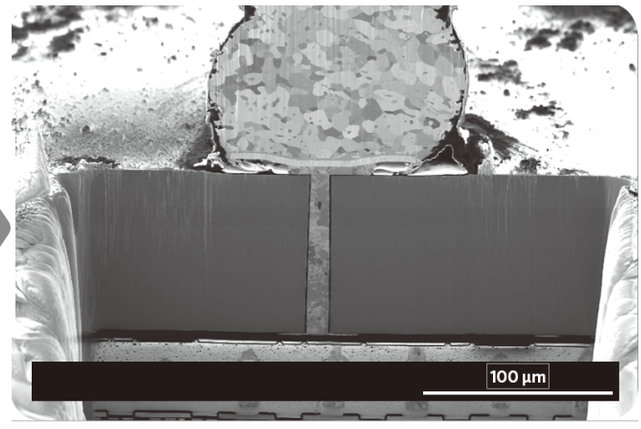

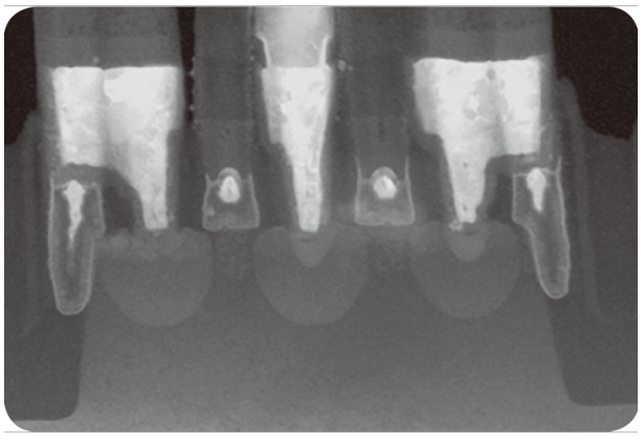

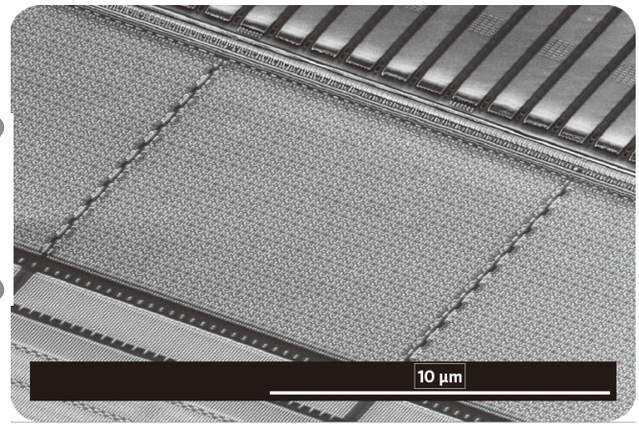

See the advantage: **FEI.com**